



Chinese Pharmaceutical Association
Institute of Materia Medica, Chinese Academy of Medical Sciences

Acta Pharmaceutica Sinica B

www.elsevier.com/locate/apbs
www.sciencedirect.com



REVIEW

Medicinal chemistry strategies towards the development of non-covalent SARS-CoV-2 M^{pro} inhibitors



Letian Song^{a,†}, Shenghua Gao^{a,b,†}, Bing Ye^a, Mianling Yang^a,
Yusen Cheng^a, Dongwei Kang^a, Fan Yi^c, Jin-Peng Sun^d,
Luis Menéndez-Arias^{e,*}, Johan Neyts^{f,*}, Xinyong Liu^{a,*},
Peng Zhan^{a,*}

^aDepartment of Medicinal Chemistry, Key Laboratory of Chemical Biology (Ministry of Education), School of Pharmaceutical Sciences, Cheeloo College of Medicine, Shandong University, Jinan 250012, China

^bShenzhen Research Institute of Shandong University, Shenzhen 518057, China

^cThe Key Laboratory of Infection and Immunity of Shandong Province, Department of Pharmacology, School of Basic Medical Sciences, Shandong University, Jinan 250012, China

^dKey Laboratory Experimental Teratology of the Ministry of Education, Department of Biochemistry and Molecular Biology, School of Basic Medical Sciences, Cheeloo College of Medicine, Shandong University, Jinan 250012, China

^eCentro de Biología Molecular “Severo Ochoa” (Consejo Superior de Investigaciones Científicas & Autonomous University of Madrid), Madrid 28049, Spain

^fKU Leuven, Department of Microbiology and Immunology, Rega Institute for Medical Research, Laboratory of Virology and Chemotherapy, Leuven 3000, Belgium

Received 11 May 2023; received in revised form 10 July 2023; accepted 2 August 2023

KEY WORDS

COVID-19;
SARS-CoV-2;
Main protease;
Non-covalent inhibitors;

Abstract The main protease (M^{pro}) of SARS-CoV-2 is an attractive target in anti-COVID-19 therapy for its high conservation and major role in the virus life cycle. The covalent M^{pro} inhibitor nirmatrelvir (in combination with ritonavir, a pharmacokinetic enhancer) and the non-covalent inhibitor ensitrelvir have shown efficacy in clinical trials and have been approved for therapeutic use. Effective antiviral drugs are needed to fight the pandemic, while non-covalent M^{pro} inhibitors could be promising alternatives due to

*Corresponding authors.

E-mail addresses: lmendez@cbm.csic.es (Luis Menéndez-Arias), johan.neyts@kuleuven.be (Johan Neyts), xinyongl@sdu.edu.cn (Xinyong Liu), zhanpeng1982@163.com (Peng Zhan).

[†]These authors made equal contributions to this work.

Peer review under the responsibility of Chinese Pharmaceutical Association and Institute of Materia Medica, Chinese Academy of Medical Sciences.

<https://doi.org/10.1016/j.apbs.2023.08.004>

2211-3835 © 2024 The Authors. Published by Elsevier B.V. on behalf of Chinese Pharmaceutical Association and Institute of Materia Medica, Chinese Academy of Medical Sciences. This is an open access article under the CC BY-NC-ND license (<http://creativecommons.org/licenses/by-nc-nd/4.0/>).

their high selectivity and favorable druggability. Numerous non-covalent M^{Pro} inhibitors with desirable properties have been developed based on available crystal structures of M^{Pro}. In this article, we describe medicinal chemistry strategies applied for the discovery and optimization of non-covalent M^{Pro} inhibitors, followed by a general overview and critical analysis of the available information. Prospective viewpoints and insights into current strategies for the development of non-covalent M^{Pro} inhibitors are also discussed.

© 2024 The Authors. Published by Elsevier B.V. on behalf of Chinese Pharmaceutical Association and Institute of Materia Medica, Chinese Academy of Medical Sciences. This is an open access article under the CC BY-NC-ND license (<http://creativecommons.org/licenses/by-nc-nd/4.0/>).

1. Introduction

In late 2019, an outbreak of a highly infectious disease with pneumonia-like symptoms (fever, dry cough, and fatigue) emerged and quickly deteriorated into a global pandemic and a major threat to global health¹. The etiological agent of the disease was the severe acute respiratory syndrome coronavirus-2 (SARS-CoV-2) and the disease was named as coronavirus disease 2019 (COVID-19). SARS-CoV-2 is a betacoronavirus that shares 82% genomic sequence identity with SARS-CoV-1, and is the seventh known coronavirus pathogenic to humans². According to the World Health Organization (WHO), there were 767 million confirmed infections and 6.94 million deaths globally in early July 2023³. Public health policy and massive vaccination are adopted as countermeasures in the battle against COVID-19 pandemic, but variants with increased transmissibility and immune resistance have become dominant among circulating viruses⁴. The Omicron variant bears dozens of mutations in the viral Spike protein, while threatening the efficacy of the vaccination program due to reduced immunological response, while hampering the effectiveness of antibody-based therapies^{5,6}. Novel SARS-CoV-2 variants with enhanced infectivity have led to additional increases in the COVID-19 transmission rate, along with a swift increase in the number of infections⁷. With no end of the battle against SARS-CoV-2 in sight, the human public health and world economy profoundly depends on effective controlling COVID-19 and future SARS-CoV-2 emerging variants. Effective direct-acting antivirals, especially oral drugs easily administered, would be a last hurdle towards a robust defense against this threatening disease⁸. Early efforts produced several repurposed drugs that entered clinical trials, including remdesivir⁹, molnupiravir¹⁰, favipiravir¹¹ and becnifosbuvir hemisulfate (AT-527)¹², but none of them has shown full effectiveness and convincing clinical efficacy^{13–18}.

The viral main protease (M^{Pro}) is one of the most attractive targets in anti-coronavirus therapy due to its high conservation, unique cleavage sequence preference and the absence of similar proteases in the host cell¹⁹. Major efforts focused on targeting M^{Pro} have led to the discovery and approval of nirmatrelvir, a reversible covalent inhibitor developed by Pfizer, and administered in combination with ritonavir, a booster of protease inhibitors that acts by inhibiting the cytochrome major P450 isoforms 3A4 and 2D6, therefore helping to maintain high drug levels for longer periods of time¹⁸. The combination of nirmatrelvir and ritonavir (commercialized as Paxlovid[®]) was approved by the U.S. Food and Drug Administration (FDA) for emergency use in December 2021 and its use has been authorized in several countries across the world. At the beginning of 2023, the Chinese National Medical Products Administration (NMPA) conditionally approved the commercialization of therapeutic drugs against

COVID-19, namely, SIM0417²⁰ and RAY1216²¹, whose chemical structures and antiviral activities are similar to that of nirmatrelvir, of which RAY1216 does not need to be combined with ritonavir.

In addition, Shionogi Inc. announced the emergency approval of ensitrelvir (S-217622) by Japanese authorities, which is the only marketed non-covalent M^{Pro} inhibitor so far²². In the meantime, non-covalent M^{Pro} inhibitors with different scaffolds are being extensively studied and developed, guided by traditional and novel medicinal chemistry strategies.

Recent reviews^{23–25} on SARS-CoV-2 M^{Pro} inhibitors mainly focus on nirmatrelvir and other covalent M^{Pro} inhibitors since this was a productive line of research during the outbreak. However, the identification of effective non-covalent M^{Pro} inhibitors came later and this area was considered to be less productive, despite being equally interesting. Insights into the non-covalent M^{Pro} inhibitors, including strategies, experience, and future directions were rarely summarized. Considering the potential advantages of non-covalent M^{Pro} inhibitors and the increasing number of reports focusing on M^{Pro} as a target, we think that it is important to compile and interpret the available information in order to provide suitable guidelines towards the discovery and development of new drugs for clinical treatment of COVID-19. Herein, we summarize a wide range of promising non-covalent M^{Pro} inhibitors obtained by using different medicinal chemistry strategies. Discussions, insights and future prospects centered on these strategies are also pursued.

2. M^{Pro}: From structural biology to drug targeting

2.1. M^{Pro} plays a key role in the replicative cycle of SARS-CoV-2

The SARS-CoV-2 genome contains 14 open reading frames (ORFs), among which ORF1a and ORF1b make up more than two-thirds of its full length²⁶. Upon invasion of host cells, the two sequences are translated into two overlapping polyproteins, pp1a and pp1ab. The pp1a contains sequences from nsp1 (non-structural protein) to nsp11, while pp1ab contains sequences from nsp1 to nsp16 (Fig. 1A)²⁷. The M^{Pro} (nsp5) and papain-like protease (PL^{Pro}, a domain of nsp3)²⁸, generated by auto-cleavage²⁹, are responsible for post-translational processing of polyproteins. M^{Pro} is a cysteine protease responsible for the proteolytic cleavage at eleven sites from nsp5 to nsp16, specifically acting on the sequence LQ↓(S/A/G). The important role of M^{Pro} in virus replication, as shown in Fig. 1B, warrants a lot of attention as a therapeutic target.

2.2. The structural features and function of M^{Pro}

2.2.1. Catalytic activity and properties

SARS-CoV-2 M^{Pro} is a polypeptide of 306 amino acids with a molecular weight of 33.8 kDa. It belongs to the C30 family of

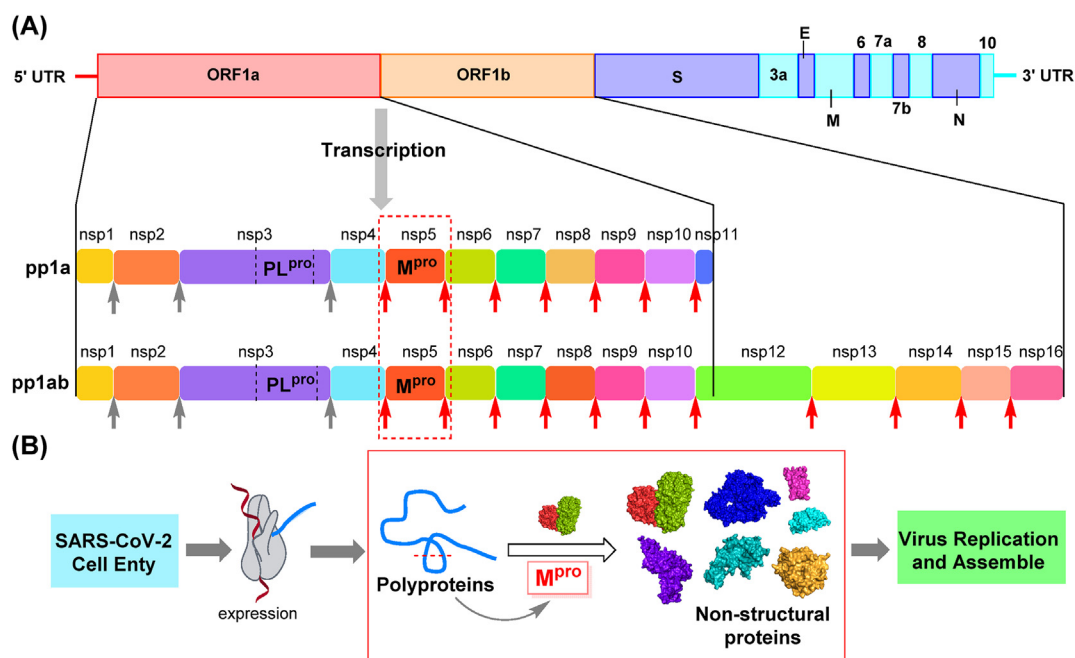


Figure 1 SARS-CoV-2 genomic organization and viral proteins. (A) Sequence of SARS-CoV-2 polyprotein; M^{pro} cleavage sites are indicated by red arrows, and PL^{pro} cleavage sites are indicated by gray arrows. (B) Diagram highlighting the role of M^{pro} in the replicative cycle of SARS-CoV-2.

proteolytic enzymes³⁰ and has a similar sequence and superimposable tertiary structure compared with previously identified SARS-CoV-1 M^{pro}^{31,32}. It contains distinct domains I (residues 8–101) and II (residues 102–184), responsible for forming the catalytic site, and the helical bundle domain III (residues 201–303) that stabilizes the protein dimer (Fig. 2A)³³. The active site of M^{pro} is a catalytic dyad formed by residues His41 and Cys145. Neutron scattering combined with X-ray to reveal a zwitterionic form of the active center, where the thiol group of Cys145 bears a stable negative charge and His41 is doubly

protonated³⁴. The proteolytic reaction catalyzed by M^{pro} initiates with the electrophilic attack of the CH₂S⁻ side chain towards the carbonyl group of peptide bond, and is followed by the hydrolysis of the resulting thioester (Fig. 2B)³⁵.

2.2.2. Active site, key residues, and two types of inhibitors

A series of sub-pockets for substrate recognition and binding are located around the catalytic center of SARS-CoV-2 M^{pro} and form the substrate-binding pocket (Fig. 3)^{36,37}. The hydrophilic cavity S1 is centered around the imidazole ring of His163, and

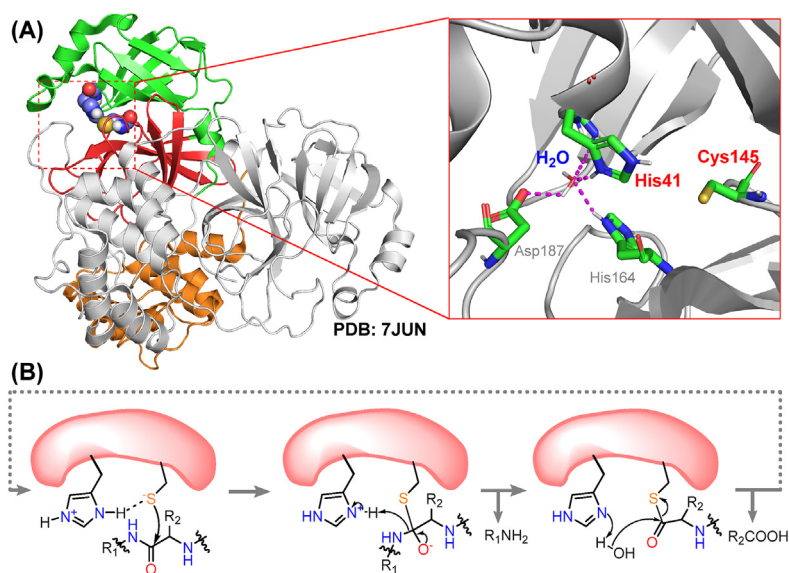


Figure 2 Structure and catalytic mechanism of SARS-CoV-2 M^{pro}. (A) Crystal structure of the M^{pro} homodimer and close-up view of its catalytic site (PDB ID: 7JUN). Domains I, II and III are represented with green, red and orange cartoons, respectively. All structures hereinafter are visualized by Pymol (pymol.org). (B) Proposed catalytic mechanism of M^{pro}.

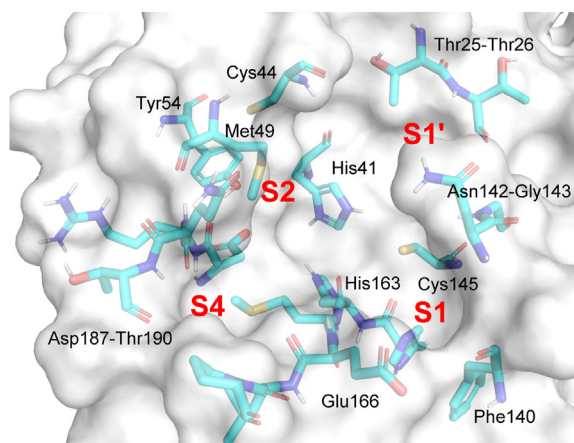


Figure 3 Residues and sub-pockets at the dimerized SARS-CoV-2 M^{pro} catalytic site (PDB ID: 7JUN). The second monomer is not shown in the figure.

surrounded by the side chains of Phe140, Leu141, Asn142 and Glu166. It shows a marked preference for CONH₂ in the side-chain of Gln as peptide substrate. S1' contains the catalytic dyad His41–Cys145, with Thr25, Thr26, Leu27 lining on the farther edge. S2 is defined by His41, Met49, Tyr54, and Met165, and is more likely to form hydrophobic and π – π stacking interactions with ligands³⁸. S4 shares the side chain of Gln189 with S2, and is lined by residues Met165, Leu167, Phe185 and Gln192. In the ligand-free state, S4 is mostly closed³⁷, but the greater flexibility of Gln189 facilitates the accommodation of various hydrophobic groups at this position^{39,40}. Those cavities described above are considered the most important sites for substrate selectivity and M^{pro} activity, as well as for binding directly-acting protease inhibitors³⁷.

The prevailing peptide-based covalent M^{pro} inhibitors bear a peptidic scaffold with highly active warheads. Electrophilic warheads can “trap” the thiol group of Cys145 through an irreversible or reversible covalent bond^{41,42}, thus inactivating the enzyme. The prevailing peptide-based covalent inhibitors bear a peptidic scaffold with highly active warheads. However, their low metabolic instability made most of these compounds only suitable for intravenous administration (*e.g.*, PF-00835231). Most of the peptidomimetic M^{pro} inhibitors could be also effective inhibitors of human cathepsins⁴³, which play significant roles in cellular metabolism. Meanwhile, the arising drug-resistant M^{pro} mutants have shown lower sensitivity to nirmatrelvir, and therefore, their spread represents a major threat to the efficacy of nirmatrelvir and related inhibitors^{44,45}.

Non-covalent inhibitors act by competitively binding to the catalytic site through critical hydrogen bonds and non-polar interactions, which may trigger distortions of the sub-pockets and displace essential water molecules, finally blocking the sub-pockets and inhibitor access to the catalytic site²⁵. The most potent non-covalent M^{pro} inhibitors occupy at least two of these cavities and build up strong interactions with multiple key residues. With reasonable means of development and modification, non-covalent M^{pro} inhibitors could avoid these problems and reach the same level of antiviral activity as covalent inhibitors. The unique advantages and diverse structural types of non-covalent M^{pro} inhibitors have led to growing interest in their development.

2.2.3. Dimer-dissociation equilibrium and inactivated state regulates M^{pro} activity

X-ray structures revealed that SARS-CoV-2 M^{pro} requires a homodimer to function properly, as observed for homologous M^{pro} enzymes of many viruses⁴⁶. The two monomers are arranged in a nearly orthogonal position, stabilized by interface residues of domain III. A salt bridge between Glu290 and Arg4' acts as the major force controlling dimerization⁴⁷. In the dimerization state, the side chain of Ser1' in the other monomer is brought near Glu166, eventually shaping the substrate binding area around S1 and S1' sub-pockets. Therefore, dimerization is a prerequisite for the normal proteolytic activity of M^{pro}^{47,48}. Small molecules, and mutations affecting Arg4, Met6, Gln11, Ser139, Glu290, Arg298 may significantly reduce the tendency of M^{pro} to dimerize and therefore impair proteolytic function⁴⁹. A recent study also revealed an inactive conformation of M^{pro} in solution, characterized by a collapsed active site and weaker interactions at the dimer surface⁵⁰. This conformation of M^{pro} provides potential targets for inhibitor design.

3. Strategies for the discovery of non-covalent M^{pro} inhibitors

Unlike covalent peptide-like inhibitors that have been widely studied clinically and even approved for therapeutic use, most of the available non-covalent M^{pro} inhibitors are at earlier stages of development. Further progress is highly dependent on the effective discovery rate of promising small-molecule leads and the rational modification of existing inhibitors. Published advances in the field result from a variety of medicinal chemistry strategies that are individually discussed in the following sections. Structural evolution, structure–activity relationships (SARs), and mode of interaction (MOI) of some representative compounds are presented all together.

3.1. Virtual screening

3.1.1. Classical virtual screening of diverse libraries

Virtual screening has been one of the most widely practiced strategies in discovering M^{pro} inhibitors. We classified representative studies by their key features, and discussed their reliability and contributions in a critical perspective. A representative example is the docking-based virtual screening of 688 compounds from a focused library of naphthoquinones⁵¹. Rigid docking, flexible docking and enzyme inhibition assay led to the identification of compound **1** (IC₅₀ = 0.40 μ mol/L, Fig. 4). Dithiothreitol (DTT) addition and dilution assays confirmed specific and reversible non-covalent M^{pro} inhibition by compound **1**, and clearly distinguished it from other non-specific inhibitors in the same study. Similarly, compounds **2–4** were discovered from commercial libraries, showing modest M^{pro} inhibitory activities (Fig. 4)^{52–54}. Apart from the general workflow of virtual screening, these studies also applied feasible and effective measures to increase accuracy and reliability. In the case of **3**, a 3D-QSAR (quantitative structure–activity relationship) model was trained by existing M^{pro} inhibitors, which led to effective hit discovery⁵³. Libraries containing approved small-molecule drugs were explored to identify compounds with acceptable safety profiles and druggability. **5** (dabigatran) and **6** (bepridil) were successively repurposed as potent SARS-CoV-2 M^{pro} inhibitors, which were discovered *via* virtual screening of the approved

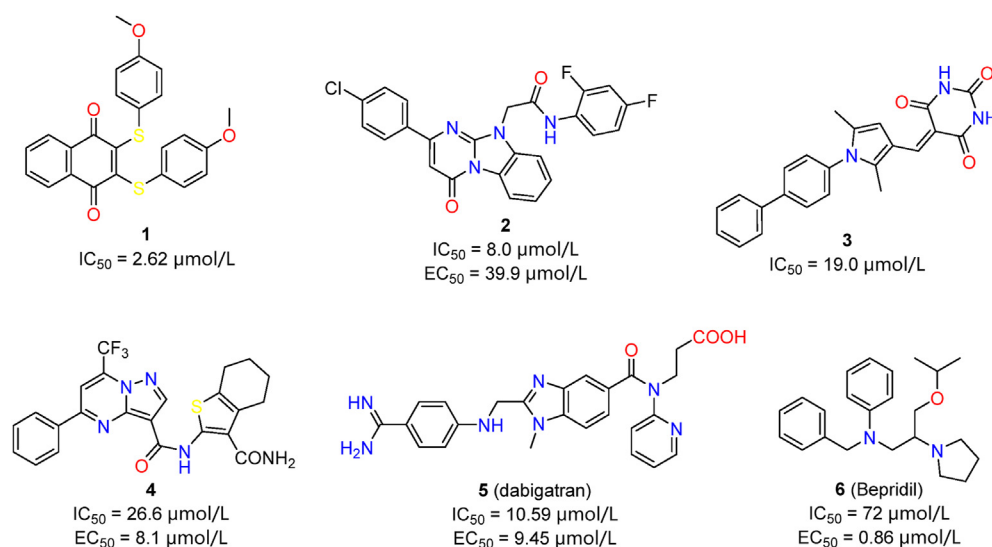


Figure 4 Verified non-covalent hit compounds from virtual screening targeting M^{Pro}.

drugs^{55,56}. The strong inhibitory activities of these two compounds demonstrate the effectiveness of this screening strategy. Repurposed drugs have higher safety and feasibility than those random molecules in compound library, therefore should receive higher attention.

3.1.2. Virtual screening combined with structural optimization

To improve activity and druggability of identified hits, modifications facilitated by virtual screening could be subsequently performed. Two compounds (**7** and **8**) with an imidazolidine-2,4-dione (hydantoin) scaffold were chosen as hits for further modifications after screening an ultra-large library containing 235 million molecules⁵⁷. As depicted in co-crystal structures, the carbonyl oxygens from **7** and **8** formed hydrogen bonds with the backbone amido group of Gly143 and Glu166, while 3- and 5-substitutions target S1 and S2 sub-pockets, respectively. Systematic exploration of substituents around the hydantoin core were pursued. Pyridine ring was proved to be optimal as S1 binder as it targeted His163 effectively, while a spiro linker joining lipophilic groups towards the S2 cavity was preferred (Fig. 5A, **9–10**). A combination of identified privileged groups led to the design of compound **11** with sub-micromolar inhibitory activity. Moreover, based on its co-crystal structure, the *ortho*-chlorophenyl group was introduced in the S2 cavity. The resulting compound **13** demonstrated a 5-fold improvement in M^{Pro} inhibitory activity (IC₅₀ = 0.077 μmol/L, Fig. 5B), along with strong anti-coronavirus activity (SARS-CoV-2: EC₅₀ = 0.11 μmol/L, SARS-CoV-1: EC₅₀ = 0.39 μmol/L, and MERS-CoV: EC₅₀ = 0.20 μmol/L). Low molecular weight and potent broad-spectrum activity make it an attractive lead compound for further evaluation. Here, efficient computing tools and large libraries play a key role in the rapid identification of hydantoin-based M^{Pro} inhibitors.

Compounds **14** and **15** were obtained from multipurpose screening against 17 targets related to COVID-19 therapy including M^{Pro}⁵⁸, and showed over 70% M^{Pro} inhibition at 40 μmol/L⁵⁹. In the screening of structure-related compounds based on an *N*-aryl-dihydroquinolinone-4-carboxamide scaffold, **16–22** were identified as potent M^{Pro} inhibitors (Fig. 6A). These compounds showed enhanced enzymatic inhibition activities

(IC₅₀ = 1.0–5.8 μmol/L). The preliminary SAR of substituent groups is depicted in Fig. 6B. The co-crystal (PDB ID: 7P2G) structure of compound **21** indicated that the dihydroquinolinone moiety makes multiple H-bonds with key residue His163 of the S1 subsite, while the oxygen of the carboxamide linker reaches Glu166 and Cys145. The iodobenzene moiety occupies the S2 cavity while making π - π stacking and strong halogen bonds with His41 and Met49, respectively (Fig. 6C). Nonetheless, compound **21** only occupied two subsites of the M^{Pro} active center. Further studies should be focused on extending this lead compound into the S1' and S4 subsites, while assessing antiviral activities in different cell lines and animal models.

An MCULE library containing 6.5 million compounds was screened using five receptor models and two docking protocols⁶⁰. Compound **23** (MCULE-5948770040) was identified as the most potent M^{Pro} inhibitor (IC₅₀ = 4.2 μmol/L). The crystal structure of **23** in complex with M^{Pro} revealed its non-covalent binding mode and full occupation of the S1 and S2 cavities (Fig. 7A). Immediately afterward, a series of compounds with the modified S1- and S2- binding groups were synthesized. These efforts resulted in the generation of two compounds (**24**, **25**) with 3,4,5-trisubstituted S2 groups that showed about two-fold increased inhibitory activity (IC₅₀ = 0.29 μmol/L, Fig. 7B)⁶¹. These piperazine derivatives are valuable lead compounds for further modification (see Section 3.3.4).

Structural modifications based on library screenings provide a shortcut to finding potential active analogs of specific hit compounds and a better interpretation of SAR. However, such a practice might be limited by the diversity, property and commercial availability of library compounds.

3.1.3. Virtual screening coupled with artificial intelligence and machine learning

Machine learning, based on previous data sets, proved to be more effective and accurate in discovering novel M^{Pro} inhibitors. Complementary QSAR and BABM (biological activity-based modeling) modules can be combined in machine learning assays for the discovery of novel drug candidates⁶². The resulting activity-based models were trained by public databases. Among the selected compounds, **26** (fluorobexarotene, Fig. 8) exhibited

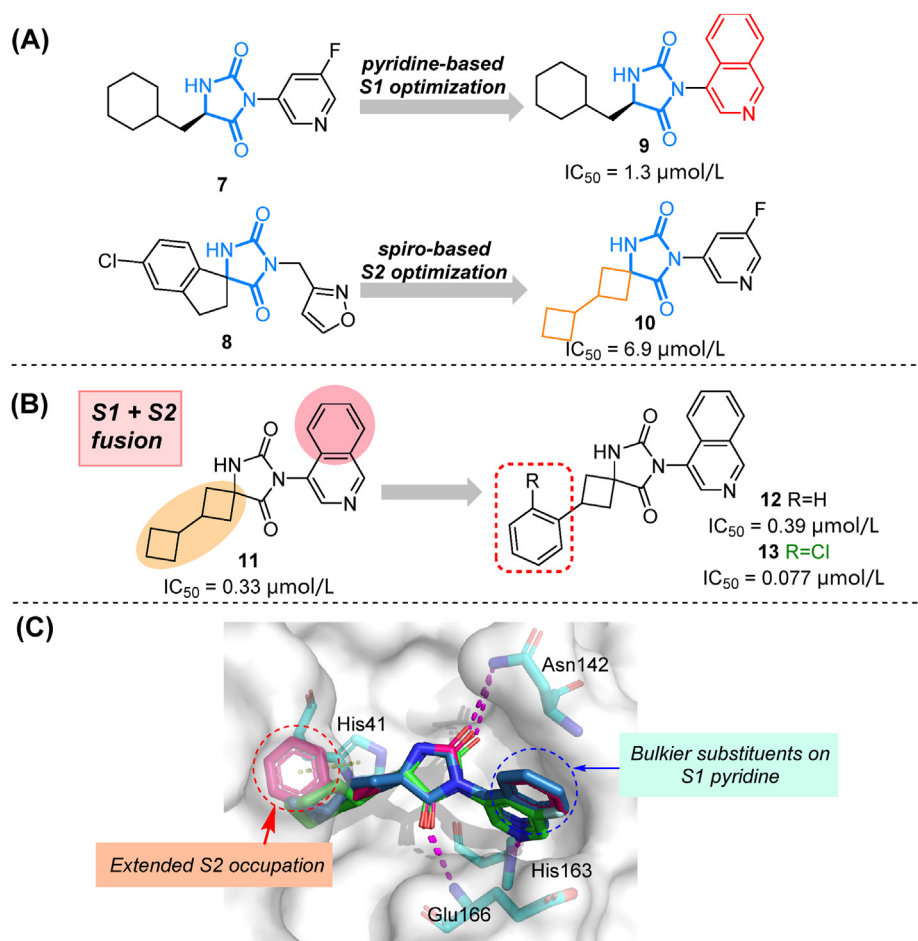


Figure 5 Screening-based modification of hydantoin-based M^{Pro} inhibitors. (A) Structures and activities of hits/compounds (**7–10**) from two rounds of screening. (B) Structures and activities of compounds **11–13**. (C) Co-crystal structures overlay and residue interactions of **7** (green, PDB ID: 7B2U), **11** (blue, PDB ID: 7O46) and **12** (magenta, PDB ID: 7QBB). Hydrogen bonds are shown as magenta dashed lines, π - π stacking are shown in green dashed lines.

moderate inhibitory activity in enzymatic assays and a cytopathic effect reduction in cell-based assays (HEK293-ACE2 cells). More importantly, this improved method showed 10.4-fold increase of the hit rate. In another effort involving the screening of a library including 40 billion compounds, candidate molecules were processed by a deep docking method driven by artificial-intelligence and pharmacophore model filtering⁶³. Automated strategy and visual inspection were combined to select potent inhibitors (represented by compound **27**, Fig. 8) with IC_{50} values around $10 \mu\text{mol/L}$. As predicted by docking results, **27** spans over at least three pockets at the M^{Pro} active center, and it is more suitable for further structural modifications. Overall, automated artificial intelligence can be helpful to avoid randomness in docking simulations, while providing more valuable hit compounds for further improvement through modifications.

3.1.4. Lessons from virtual screening campaign

From the examples presented in the previous sections, we conclude that the outcome of virtual screening depends on several factors. Improving the predictability of the docking method is of utmost importance. For instance, considering the adaptability of the M^{Pro} active site, receptor-flexible docking methods could be used to better predict ligand binding pattern⁶⁴. A compound

library with superior quantity and quality, a series of reasonable filters to remove undesired compounds and an evaluation system that better predicts ligand affinity are also indispensable. Experimental measurement of biochemical activity should be conducted, not only for validation, but also for demonstrating the correlation between predicted properties and compound activities^{65,66}. Unfortunately, there are published studies with low-quality compounds and questionable data, which should be handled with caution. Those inhibitors bearing unstable structures or unspecific binding groups should not be considered for further development. The expanded size of virtual libraries may also lead to higher rate of false-positive compounds and fewer bioactive molecules⁶⁷. In this scenario, future *in silico* screenings should learn from the past and avoid any conclusions without concrete experimental proof to assure integrity and reliability.

3.2. High-throughput screening

Compared with computational screening, high-throughput screening (HTS) provides reliable results based on experimental data from specific assay systems. HTS was a fruitful strategy for the identification of both covalent and non-covalent M^{Pro} inhibitors⁶⁸.

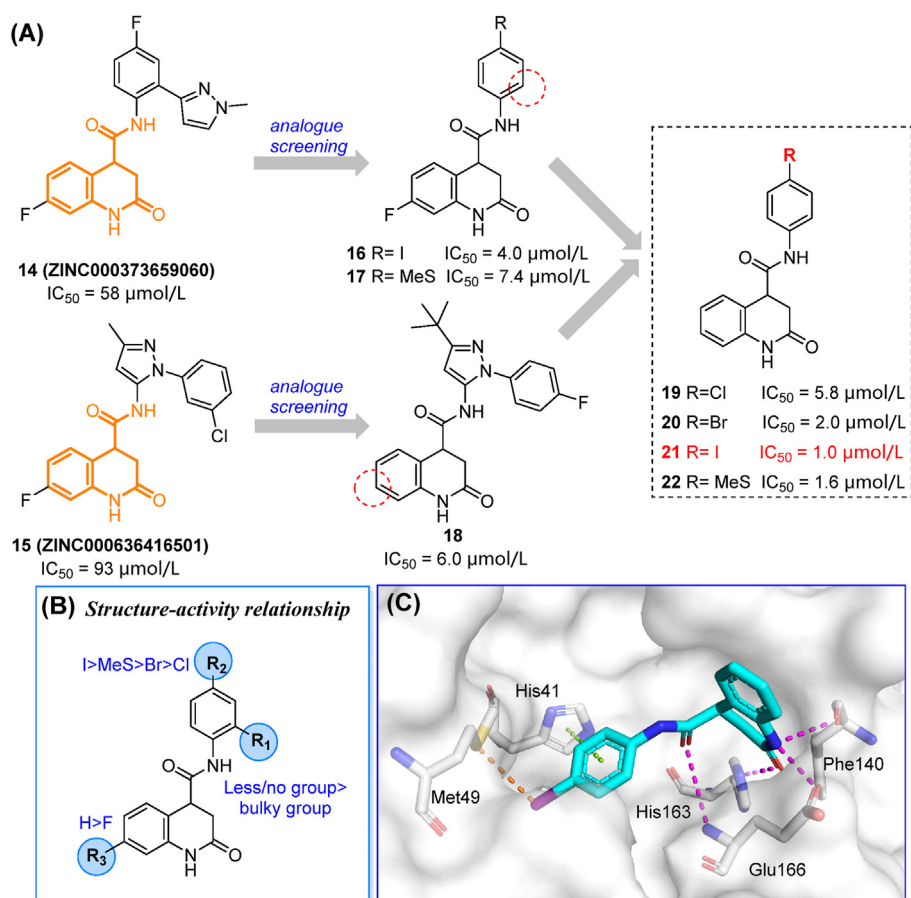


Figure 6 The discovery, optimization, and co-crystal study of dihydroquinolinone derivatives. (A) Starting hits and their screening-based optimization. (B) Preliminary SAR of the screened compounds. (C) Co-crystal structure of compound **21** and M^{pro} demonstrating space occupancy and residue interactions (PDB ID: 7P2G). Hydrogen bonds are shown as magenta dashed lines. π - π stacking are shown in green dashed lines. Halogen bonds are shown in orange dashed lines.

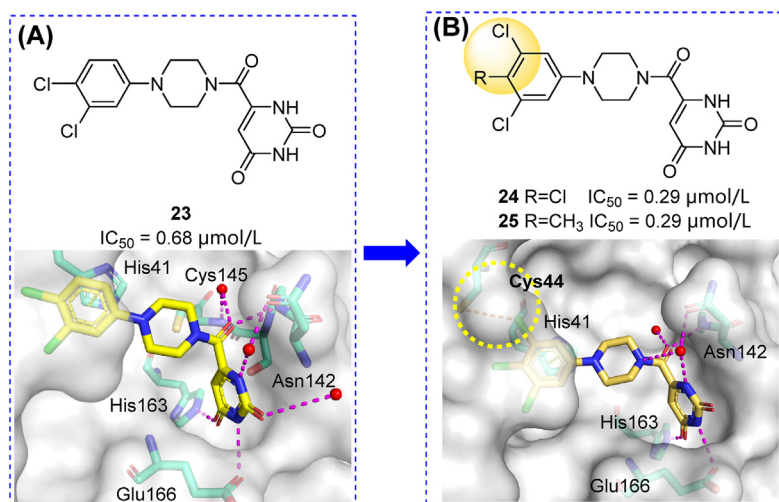


Figure 7 Structures, activities and co-crystal analysis of compounds **23** (A, PDB ID: 7LTJ) and **24** (B, PDB ID: 7RLS). Hydrogen bonds are shown as magenta dashed lines. π - π stacking are shown in green dashed lines.

3.2.1. Advances in HTS aimed at the identification of M^{pro} inhibitors

FRET (fluorescence resonance energy transfer) is the most typical assay for M^{pro} inhibitor screening. A peptidic substrate containing

a fluorogenic group connected with quencher by linker sequence can be recognized by M^{pro}. Cleavage of the peptide linker leads to a detectable shift in the emission wavelength. Thus, enzymatic inhibition could be determined from the intensities of emission at two

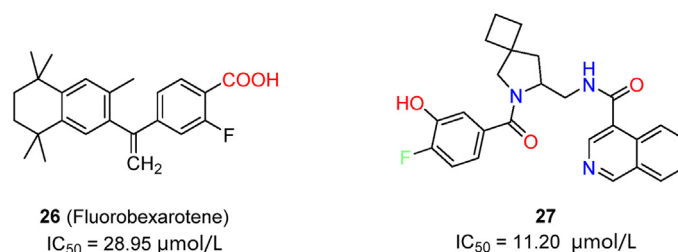


Figure 8 Hit compounds discovered with the assistance of artificial intelligence and machine learning.

different wavelengths⁶⁹. FRET-based assays can be further modified and improved to prevent misidentification of false-positive compounds while increasing assay sensitivity^{70,71}. Analogously, a protein biosensor obtained by linking the fluorescent proteins eCFP (cyan fluorescent protein) and Venus (a yellow fluorescent protein) through the peptide sequence TSAVLQ↓SGFRK, which could be hydrolyzed by M^{pro} at the cleavage site (marked with the arrow “↓”), have been developed⁷². The luminescence-based assay⁷³ involves the use of amnioluciferin which is released from a peptide probe by M^{pro}, and converted to a light signal by luciferase. This novel assay provided accurate measurements of IC₅₀ values for M^{pro} inhibitors, and is a potential choice for HTS. Moreover, cell-based virus-free HTS assays are also widely used. FlipGFP (green fluorescent protein), cell lysate Protease-Glo luciferase and luciferase complementation assays were also reported as effective methods for the screening of M^{pro} inhibitors^{74,75}. Cell-based HTS systems are encoded to express M^{pro} and probe proteins with an M^{pro} cleavage site. Upon M^{pro} cleavage, the light signal provided by the experimental system shows detectable changes, which reflect the relative activity of protease. Such systems could be helpful to rule out problematic compounds with high toxicity or low permeability.

3.2.2. Non-covalent M^{pro} inhibitors identified by HTS

A quantitative HTS over 10,755 compounds was practiced using FRET assays. Among them, compound **28** (walrycin B)

demonstrated remarkable inhibitory activity against M^{pro} (IC₅₀ = 0.26 μmol/L, Fig. 9A), but was cytotoxic to Vero E6 cells (EC₅₀ = 3.55 μmol/L, CC₅₀ = 4.25 μmol/L)⁷⁶. High toxicity made it useless as a therapeutic agent but could be tackled by rational modifications. Using a GFP cell-based assay, the quinazoline derivative **29** (QZ4, IC₅₀ = 6.5 μmol/L, Fig. 9A) was identified from a small in-house library. The compound showed prominent activity in the GFP assay, similar to that of boceprevir⁷⁷.

Cell-based HTS has also been helpful for drug repurposing of non-covalent M^{pro} inhibitors. Representative compound **30** (masitinib) showed an EC₅₀ of 2.1 μmol/L in an anti-coronavirus screening using HCoV-OC43 as a surrogate, while inhibiting SARS-CoV-2 with an EC₅₀ of 3.2 μmol/L (A549 cells). Further structural studies also confirmed that masitinib was a potential M^{pro} inhibitor (Fig. 9B)⁷⁸. Collectively, HTS is a practical and reliable method for identifying non-covalent inhibitors of M^{pro}. Great improvements in screening methodologies, combined with high-quality libraries are major contributors to these developments.

Novel resources, such as a DNA-encoded library (DEL) were also effectively applied in HTS of M^{pro} inhibitors. A typical DEL is based on a cocktail of millions to billions of mixed compounds, each of them labeled by specific DNA sequences. M^{pro} was immobilized on magnetic beads. After co-incubation, active compounds immobilized on beads (solid phase) were separated and decoded to determine their chemical structures. Four promising candidates (**31–34**) were identified from a DEL containing

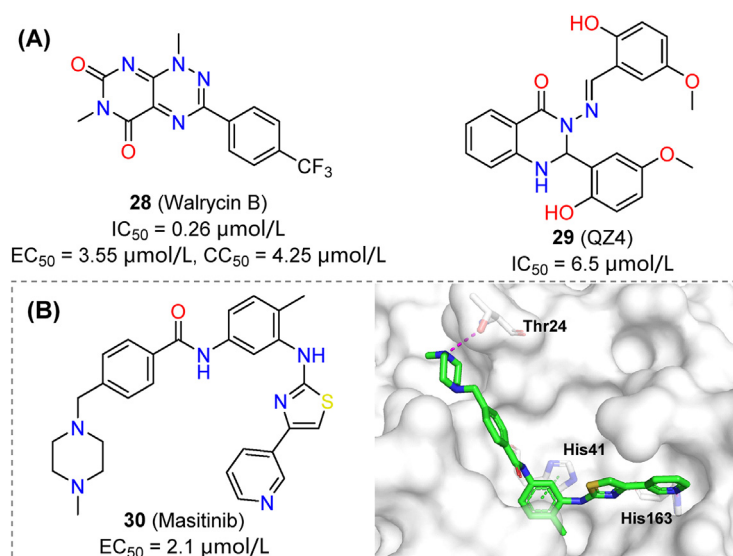


Figure 9 Non-covalent SARS-CoV-2 M^{pro} inhibitors identified by HTS. (A) Chemical structures and activities of compounds **28** and **29**. (B) Chemical structure, activity and crystal structure of **30** in complex with SARS-CoV-2 M^{pro} (PDB ID: 7TVX).

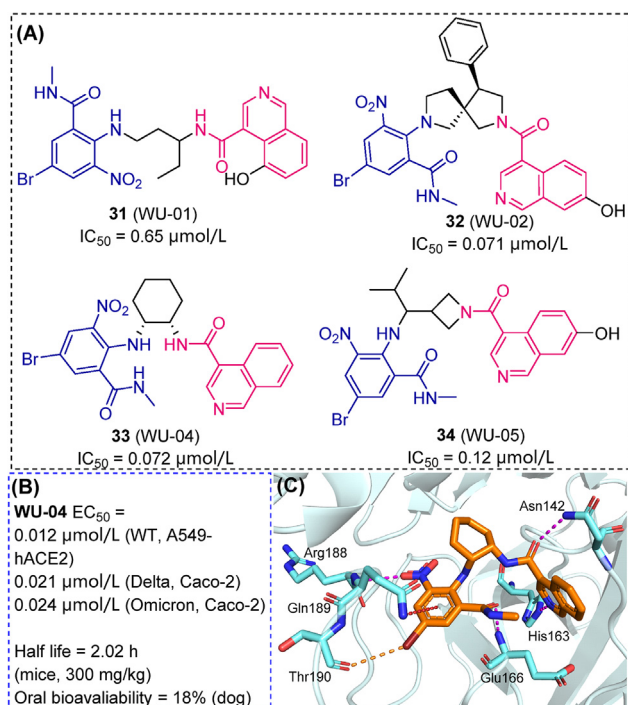


Figure 10 Hit compounds from DEL-based M^{PRO} inhibitor screening. (A) Chemical structures and IC₅₀ values of **31–34**. Common structures are highlighted in purple/blue. Chiralities of **31** and **34** are unspecified. (B) The antiviral activity towards various strains, *in vivo* half-life and oral bioavailability of **33**. (C) Residue interactions of **33** revealed by its co-crystal structure with SARS-CoV-2 M^{PRO} (PDB ID: 7EN8). Hydrogen bonds are shown as magenta dashed lines. π – π stacking are shown in green dashed lines. Halogen bonds are shown in orange dashed lines. Amnio– π interactions are shown in red dashed lines.

49 billion compounds, showing sub-micromolar IC₅₀ values against SARS-CoV-2 M^{PRO} (Fig. 10A)⁷⁹. Compound **33** (WU-04) displayed stronger antiviral activity than nirmatrelvir against the SARS-CoV-2 Omicron variant (Caco-2 cell line, 24 nmol/L *versus* 33 nmol/L, Fig. 10B), which binding mode with M^{PRO} was revealed using crystallographic methods (Fig. 10C). In mice models, twice-a-day oral dosing (300 mg/kg per dose) of **33** reduced viral load in lungs below the detection limit, and an effect on lung inflammation was also observed. DEL screening has a huge advantage in efficacy and compound diversity. Stemmed from “split-and-pool” method of generating DEL libraries, a huge number of serial analogs based on certain scaffolds can be synthesized and screened⁸⁰, therefore contributing to the optimization of potent hits targeting M^{PRO}.

3.3. Target-based rational drug design

3.3.1. Molecules generated through the Ugi reaction

The first crystal structure of SARS-CoV-2 M^{PRO} was released in early 2020, opening the door to structure-based drug design⁶⁹. The promising SARS-CoV-1-M^{PRO} non-covalent inhibitor **35** (also known as ML188) was repurposed against SARS-CoV-2 M^{PRO}⁸¹. Compound **35** had similar inhibitory activity against SARS-CoV-2 M^{PRO} (IC₅₀ value of 10.96 μmol/L) than against SARS-CoV-1 M^{PRO} (IC₅₀ = 11.23 μmol/L) (Fig. 11A)⁸². ML188 derivatives were designed by a step-wise optimization procedure and obtained through the Ugi four-component reaction. SAR studies indicated that the largest substituent that could be accommodated in the S2

sub-pocket was a biphenyl group, while the (*S*)- α -methylbenzyl moiety was preferred at the S4 subsite. Favorable substitutions at each subsite were combined, leading to compound **36** (IC₅₀ = 0.31 μmol/L) with a 54-fold improvement in the enzymatic inhibitory activity against SARS-CoV-2 M^{PRO} relative to the lead **35**. Besides, **36** exhibited potent antiviral activity towards SARS-CoV-2 in cell-based assays (EC₅₀ in Vero E6 cells of 1.27 μmol/L), without significant cytotoxicity (CC₅₀ > 100 μmol/L, Fig. 11A). As a non-covalent inhibitor, **36** was highly selective against human proteases. As revealed by the co-crystal structure of M^{PRO} and **36** (PDB ID: 7KX5, Fig. 11B), the inhibitor reached the lipophilic surface of the S2 and S4 sites through its bulkier phenyl groups and showed an extended occupation, while conserving key H-bond interactions⁸³.

The Ugi four-component reaction was also applied to the introduction of substituents at five sites of the 1,4,4-trisubstituted piperidine scaffold (Fig. 12A)⁸⁴. Multiple series of compounds were pre-screened in antiviral assays with HCoV-229E, and potent candidates were evaluated for their anti-SARS-CoV-2 activity. Notably, compound **37** (Fig. 12B) displayed an EC₉₀ value towards SARS-CoV-2 as low as 1.7 μmol/L. Multi-component reaction has been proved as a powerful chemical tool for the fast library-building and derivatization of different series of M^{PRO} inhibitors.

3.3.2. Triaryl pyridiones

Perampanel (**38**), an FDA-approved antiepileptic drug, showed relatively poor inhibitory activity against SARS-CoV-2 M^{PRO}

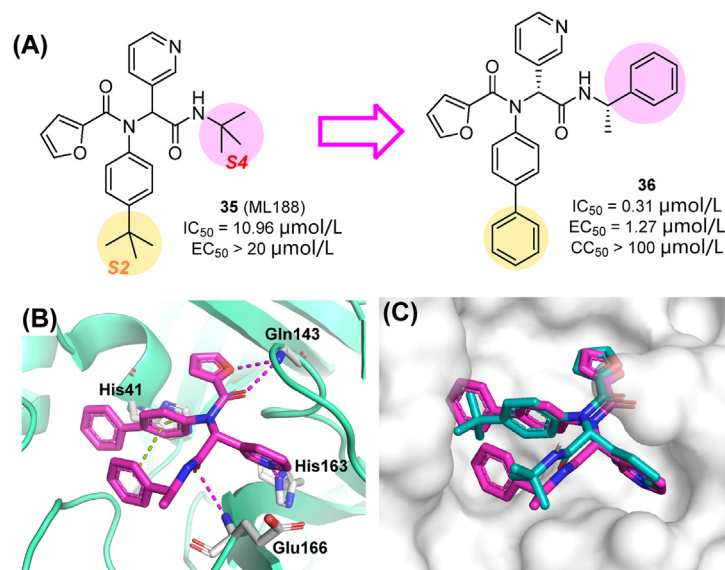


Figure 11 (A) Structures and activities of **35** and **36**. (B) M^{pro} binding mode revealed by X-ray crystallography. **36** (magenta)/**35** (cyan). Hydrogen bonds are shown as magenta dashed lines. π - π stacking are shown in green dashed lines (PDB ID: 7KX5).

($IC_{50} = 100$ – $250 \mu\text{mol/L}$), while showing non-covalent binding⁸⁵. Its stereostructure is characterized by a clover-like pattern made by three aromatic rings around a pyridone core that facilitates binding into the S1/S1'/S2 subsites. A significant improvement of activity was achieved by switching the pyridine group to S1 subsite and adding chlorine atoms to the S2 phenyl ring (see compound **39** in Fig. 13A). Further modifications were conducted to investigate the uncharted chemical space in S4 by introducing alkyl, benzyl and heterocycle groups^{86,87}. The resulting compound **40** was one of the most potent derivatives ($IC_{50} = 0.020 \mu\text{mol/L}$) in enzymatic assays. Co-crystal structures of M^{pro} in complex with perampanel analogues indicated that hydrophobic interactions in S4 could substantially affect their inhibitory activity (Fig. 13B)⁸⁸. However, **40** has no detectable antiviral activity in cell-based assays, presumably due to the poor cell permeability of uracil groups. As a countermeasure, the S1' uracil was *N*-methylated (**41**, Fig. 13A), leading to a remarkable improvement of antiviral activity *in vitro* ($EC_{50} = 0.175 \mu\text{mol/L}$). It should be noted that compound **41** has high aqueous solubility and low cytotoxicity in Vero E6 cells ($CC_{50} > 32.5 \mu\text{mol/L}$)⁸⁷.

3.3.3. Benzotriazoles

In an early effort aiming to discover non-covalent SARS-CoV-1 M^{pro} inhibitors, lead **42** was optimized to obtain **43** (ML300, $IC_{50} = 4.99 \mu\text{mol/L}$) and **44** (17b, $IC_{50} = 0.95 \mu\text{mol/L}$, Fig. 14A)⁸⁹. The two compounds extended to the S2c channel, a hydrophilic region next to canonical S2 pocket (S2sp)⁹⁰. In an effort to target SARS-CoV-2 M^{pro} , the thiophene (in S2c) and pyridine-3-yl (in S2sp) moieties of **44** were modified (Fig. 14B), while the benzotriazole-1-yl acetamide in S1 was conserved. This led to compounds **45** and **46** that increased their inhibitory activity about 8 times in comparison with **44**. The pyrazole group, acting as hydrogen bond donor at the S2c site, produced a significant improvement in the inhibitory activity. Then, the optimal groups in S2c/S2sp subsites were combined to obtain compound **47** (CCF981), that showed the strongest antiviral activity against SARS-CoV-2 in Vero E6 cells ($IC_{50} = 0.068 \mu\text{mol/L}$,

$EC_{50} = 0.497 \mu\text{mol/L}$), comparable to that of remdesivir ($EC_{50} = 0.34 \mu\text{mol/L}$). The comparison of the co-crystal structures of **47** and **43** revealed closer contacts with the S2c cavity through dual H-bonds with Cys44 and Thr25 in compound **47** (Fig. 14C and D), proving that H-bond donors are preferred in the S2c cavity. Unfortunately, the unchanged benzotriazole group was easily metabolized, requiring modifications to improve its druggability.

Fragment **48**, as a weak binder of M^{pro} , was identified from a fragment screening by X-ray crystallography⁹¹, and chosen for hit-to-lead optimization⁵⁷. This compound showed low affinity in SPR (surface plasmon resonance) assays ($K_D > 200 \mu\text{mol/L}$) and no enzymatic inhibition at $50 \mu\text{mol/L}$, but showed a good occupation of the S1 and S2 subsites. The aromatic heterocycles in the S1 cavity and the amide group directly interacting with Glu166 were conserved. More than 10 billion analogs of **48** were virtually screened and validated. The results suggested that the benzotriazole ring was preferred in the S1 subpocket. For the S2 subsite, the introduction of thiophene-fused piperidine led to the potent hit compound **49** (Fig. 15), which unexpectedly showed a strong similarity with compound **42**. In further optimization of **49**, the privileged groups in S2c could be fused onto the piperidine ring, obtaining promising compounds with novel scaffolds.

3.3.4. 1,2,4-Trisubstituted piperazines

The hit compound **23** (MCULE-5948770040), was taken as a lead compound in the rational design of highly potent and selective M^{pro} inhibitors^{60,92}. Considering that **23** only occupied two subsites in the M^{pro} active center, a side arm was added to the piperazine scaffold to occupy S4 subsite while reaching the key residue Glu166 for additional interaction. The resulting compound **50** (GA-17S) showed a 10-fold increase in M^{pro} inhibitory activity ($IC_{50} = 0.4 \mu\text{mol/L}$). However, **50** failed to show significant anti-SARS-CoV-2 activity in cell-based assays. This unexpected situation is assumed to be a consequence of the poor membrane permeability of the uracil group in S1, as discussed in section

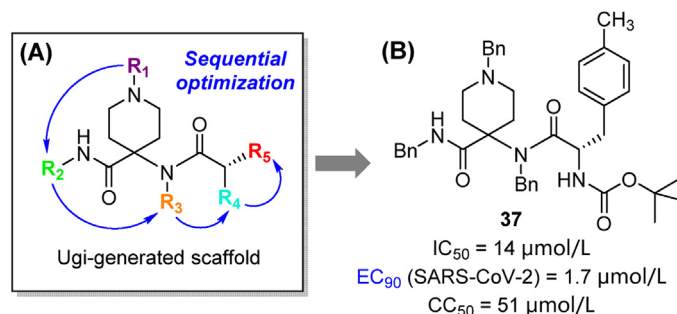


Figure 12 Discovery of the trisubstituted piperidine analogs. (A) Rational design based on Ugi-generated scaffold; (B) Structure and activity of representative compound **37**.

3.3.2. Further medicinal chemistry efforts were pursued to replace the uridine moiety. Compound **51** (GC-14) with a nicotinoyl group retained potent enzymatic inhibition, while showing remarkably enhanced antiviral activity in cell-based assays ($IC_{50} = 0.4 \mu\text{mol/L}$, $EC_{50} = 1.1 \mu\text{mol/L}$, Vero E6 cells). Compound **51** has no significant cytotoxicity at $100 \mu\text{mol/L}$, and no inhibitory activity against host proteases at $50 \mu\text{mol/L}$ (Fig. 16A). According to crystallographic studies, the newly introduced carboxamide groups in both compounds formed new hydrogen bonds with Glu166, while the terminal (thiophen-2-yl)-methyl group occupied the hydrophobic S4 subpocket. Thiophene/phenyl rings in S4/S2, together with the imidazole side-chain of His41 formed a sandwich-like stacking complex, which positioned the inhibitor in a favorable conformation, therefore increasing its affinity for the targeted protease (Fig. 16B and C). As the study highlighted, the occupation of multiple subpockets and effective interaction with key residues are critical issues to consider while developing novel M^{PRO} inhibitors.

3.3.5. S-217622 (ensitrelvir)

Ensitrelvir (S-217622) was identified as a non-covalent inhibitor of the SARS-CoV-2 M^{PRO} ($IC_{50} = 0.013 \mu\text{mol/L}$), and a promising oral drug candidate by Shionogi Pharmaceutical Research Center^{93,94}. The hit compound (**52**) was identified from an in-house

compound library, and then modified through a structure-based drug design strategy, targeting pockets S1', S1 and S2 of M^{PRO} in a stepwise manner. Cyclization of S1/S1'-interacting groups and rearrangement of fluorine atoms in the S2-binding moiety enhanced target affinity, leading to compound **53** and the drug candidate S-217622 (**54**). S-217622 displayed potent antiviral activity *ex vivo* against wild-type SARS-CoV-2 ($EC_{50} = 0.37 \mu\text{mol/L}$) and several clinical variants ($EC_{50} = 0.29\text{--}0.50 \mu\text{mol/L}$, Fig. 17A), as well as the Omicron subvariants BA.4 and BA.5. Favorable pharmacokinetic profiles in monkeys were also observed for the selected compound (CL = 0.29 mL/min/kg ; $t_{1/2} = 10.0 \text{ h}$; $F = 106\%$). In comparison with nirmatrelvir, S-217622 showed increased antiviral potency in mice⁹⁵ and hamsters⁹⁶, and ensured a 100% post-infection survival rate over 14 days (0% in those not receiving the compound)⁹⁵. Inhibitory activity against host-cell proteases was not observed, indicating the high target specificity of the candidate. Ensitrelvir was approved in Japan after the completion of phase IIa and IIb clinical trials in February 2022, becoming the first marketed non-covalent M^{PRO} inhibitor⁹⁷. A recent report has demonstrated that ensitrelvir treatment leads to a rapid reduction of SARS-CoV-2 viral loads while ameliorating the symptoms of COVID-19⁹⁸.

Co-crystal structures of M^{PRO} in complex with the hit compound **52** (Fig. 17B) and S-217622 (Fig. 17C) have been

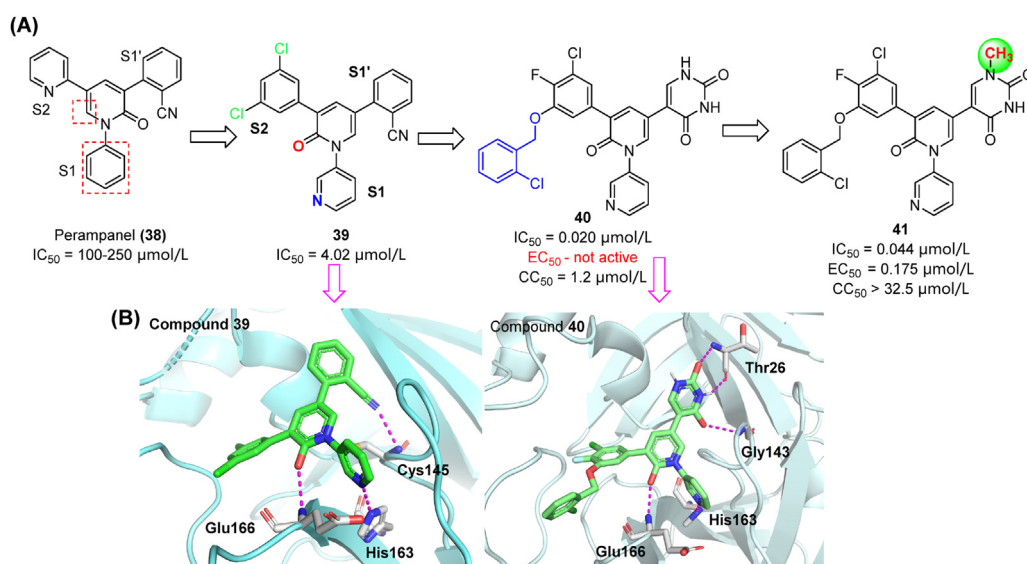


Figure 13 Discovery and co-crystal studies of perampanel derivatives. (A) Optimization process starting from compound **38**. (B) Co-crystal structure of compounds **39** (left) and **40** (right) with M^{PRO} illustrating H-bond interactions (magenta) and spatial occupancy (PDB ID: 7L10).

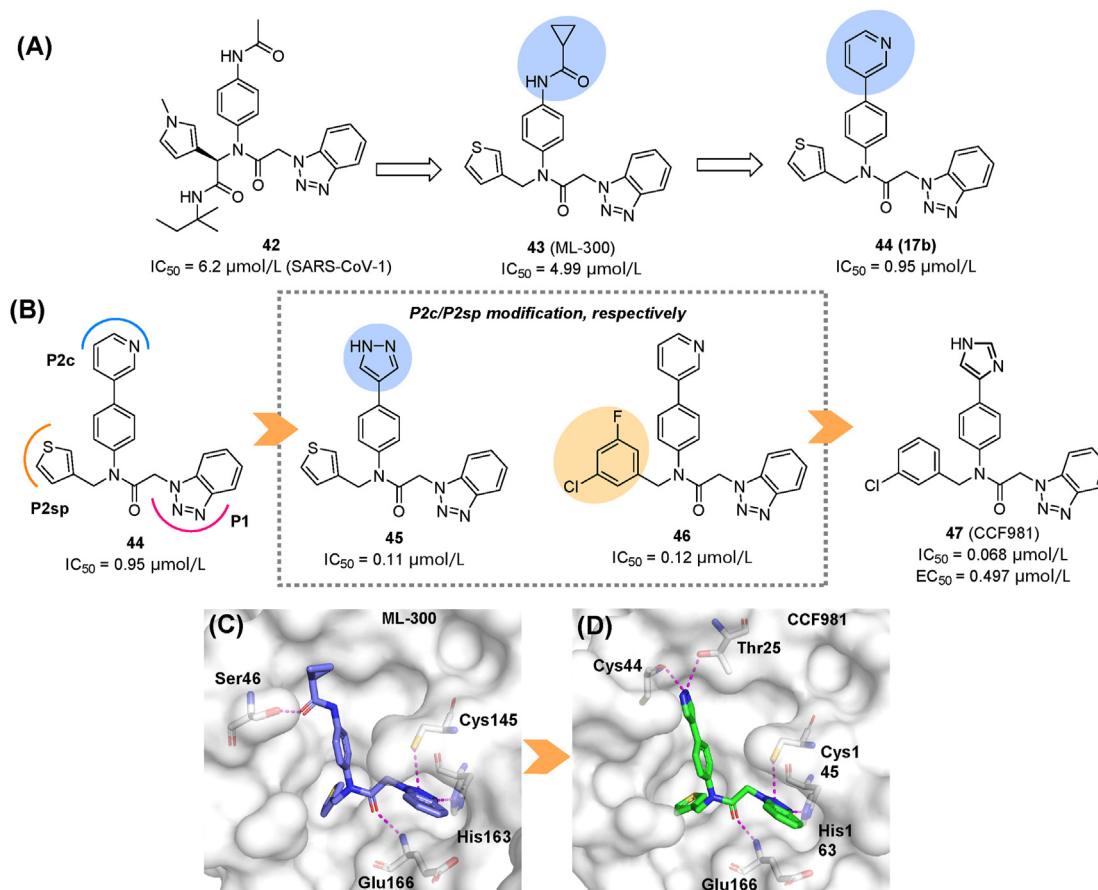


Figure 14 Modifications of benzotriazole derivatives. All the IC_{50} values presented are for SARS-CoV-2. (A) Prior modifications led to compounds **43** and **44**. (B) Rational design based on **44**. (C, D) The co-crystal structure of **43** (C, PDB ID: 7LME) and **47** (D, PDB ID: 7LMD) in complex with M^{pro} . Hydrogen bonds are shown as magenta dashed lines.

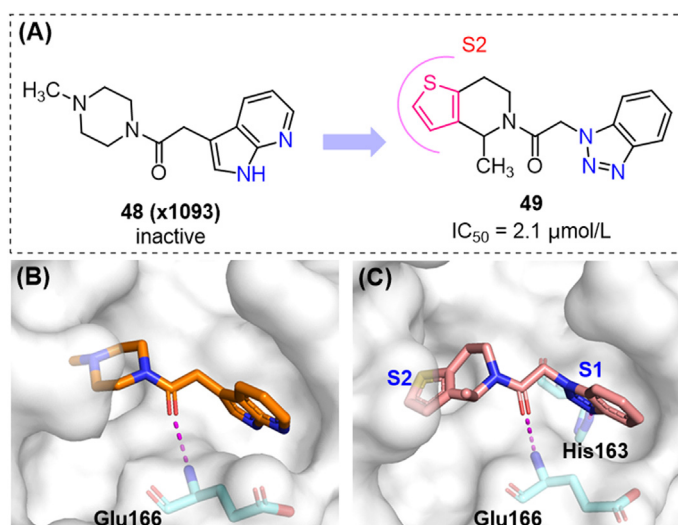


Figure 15 Optimization of fragment **48**. (A) Structures and activities of compounds **48**, **49**; (B) (C) Co-crystal structures of **48/49** with SARS-CoV-2 M^{pro} (PDB ID: 5RF7 and 7NBT).

determined. The optimized S-217622 retained an identical binding pose to that shown by compound **52**, and occupied the S1, S2 and S1' sub-pockets (Fig. 17D). The 2,4,5-trifluorobenzyl substituent fits to the hydrophobic S2 sub-pocket, stacked with

imidazole ring of His41, while the 1,2,4-triazole moiety formed a hydrogen bond with His163 in the S1 subsite. The indazole moiety occupied the S1' sub-pocket and enabled the formation of a hydrogen bond with the backbone of Thr26. Yet another

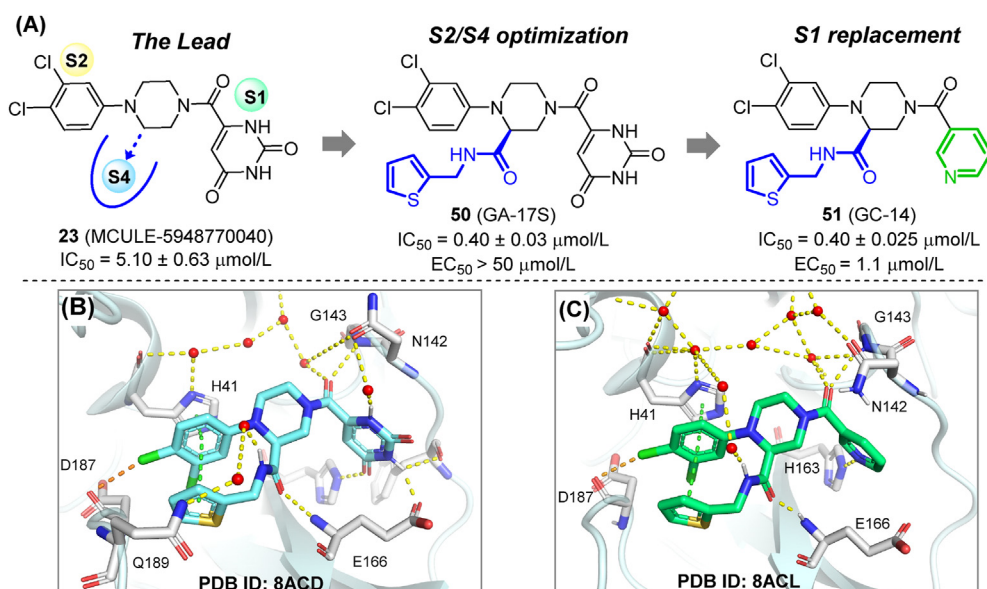


Figure 16 Rational design and co-crystal study of trisubstituted piperazine M^{Pro} inhibitors. (A) Structure and activity of **50** and **51**. (B) Co-crystal structure of **50** with SARS-CoV-2 M^{Pro} (PDB ID: 8ACD). (C) Co-crystal structure of **51** with SARS-CoV-2 M^{Pro} (PDB ID: 8ACL). Hydrogen bonds are shown as magenta dashed lines. π - π stacking are shown in green dashed lines. Halogen bonds are shown in orange dashed lines.

appealing fact is that the bulky 6-chlorine atom pushed against His41 side chain, leading to a flip of the imidazole ring. This displacement is stabilized by an additional H-bond with His41 and Tyr54, which was not observed in the apo-M^{Pro} structure (Fig. 17C). The flip leads to a reduced S2 accommodation space, but renders a close distance between the imidazole ring and 1,2,4-trifluorophenyl moiety, thereby facilitating the formation of π - π stacking interactions. Moreover, multiple hydrogen bonds were

built among the heterocyclic scaffold involving residues Glu166, Gly143, and Cys145.

3.4. Fragment-based screening and optimization

Fragment-based drug discovery (FBDD) is a strategy that emerged in recent decades. It starts with the identification of a variety of fragments, *i.e.*, weak binders of a specific target with lower

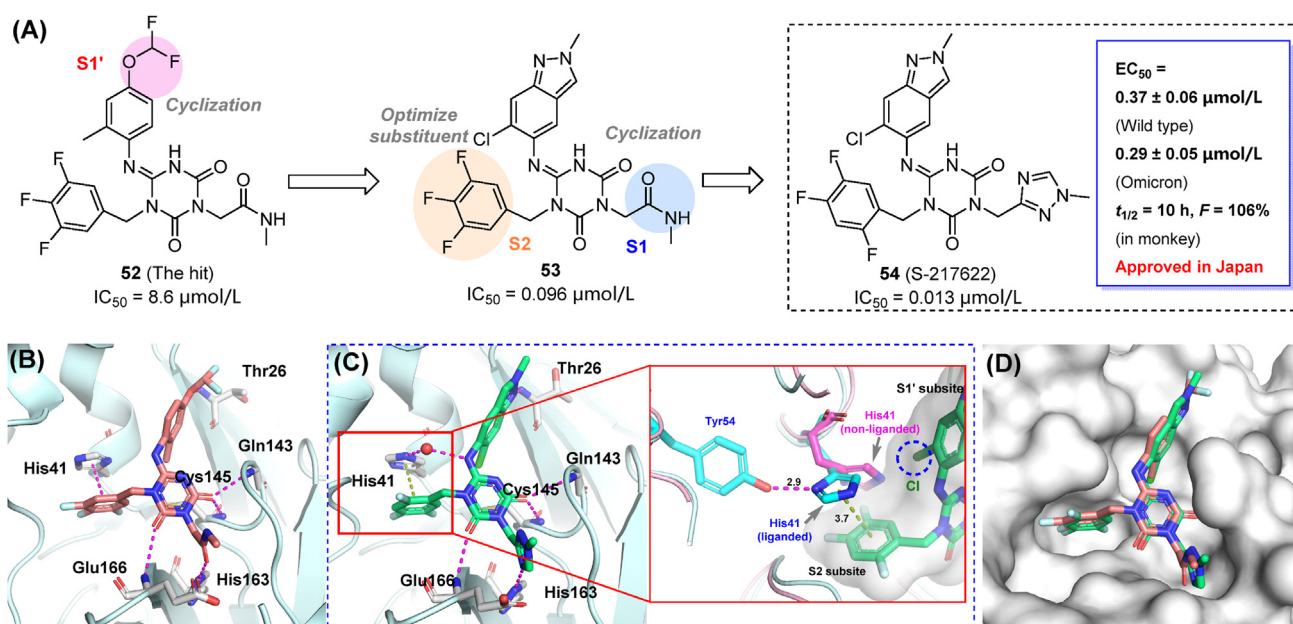


Figure 17 Design and development of ensitrelvir (**54**, S-217622). (A) Structural optimization and representative compounds in the development of ensitrelvir. (B) Co-crystal structure of compound **52** (hit) with M^{Pro}. (C) Co-crystal structure of ensitrelvir with M^{Pro} and close-up view showing the conformational change of His41. (D) Binding pose comparison of compounds **52** and **54**. Hydrogen bonds are shown as magenta dashed lines. π - π stacking are shown in green dashed lines.

molecular weight and fewer H-bond donor/acceptors than drug-like molecules. Three key factors are involved in the FBDD process: fragment libraries, screening methods and fragment modification strategies⁹⁹. FBDD has unique distinctions and superiorities compared to traditional screening and has been a tremendous aid to the discovery and approval of new drugs.

3.4.1. Screening of fragments targeting SARS-CoV-2 M^{pro}

A massive screen of both covalent and non-covalent fragments targeting M^{pro} was set out from Diamond Light Source⁹¹. A new resolving method named pan-DDA (pan-Dataset Density Analysis) was applied in the co-crystal resolution of fragments, which could interpret signals from the electron density of low-occupying ligands¹⁰⁰. As a result, a variety of non-covalent fragments and their binding poses in the protease active site were identified, along with some electrophilic fragments acting non-covalently (x0967, **55**, PDB ID: 5RG1).

Alignment analysis showed that fragments spread over the three major sub-pockets of M^{pro} (Fig. 18B–D), although the preferred binding site of each individual fragment was variable. The S1 cavity was occupied by **56** (x0434, PDB ID: 5R83) and eight other fragments containing the 3-amniopyridinyl moiety, with concurrent interactions with His163, Glu166 and even His41. In the S2 subsite, rigid aromatic rings were absolutely preferred for their π – π stacking with the His41 side chain, and their

hydrophobic interaction with Met49. The S4 cavity also favors hydrophobic fragments. These fragments showed a broad chemical space for merging and modification. A follow-up study confirmed **57** (SX013, PDB ID: 5RHD) as a fragment that binds to the M^{pro} active site, and showing an EC₅₀ value of 304 $\mu\text{mol/L}$ ¹⁰¹.

NMR is also a powerful tool for M^{pro} fragment screening¹⁰². In NMR assays, effective binding of fragments leads to a shift of the 2D-correlation signal of M^{pro} ¹H and ¹⁵N. This type of studies led to the identification of the top hit **58** (F01), which was then evaluated in enzymatic and cell-based assays and co-crystallized with M^{pro} (Fig. 19). The compound showed a relatively weak activity with an IC₅₀ value of 54 $\mu\text{mol/L}$ and an EC₅₀ value of 150 $\mu\text{mol/L}$. Considering that most fragments are too small to present measurable biological activity, **58** could be considered as potentially useful for further development.

3.4.2. Fragment-to-lead optimization

The COVID Moonshot initiative is a collaborative open-science project that uses high-throughput X-ray fragment screening to identify novel active hits against SARS-CoV-2 M^{pro}. The fragment **59** (TRY-UNI-714a760b-6, Fig. 20) was identified and chosen as the starting point for further modification in this initiative, and the results have been published in a preprint server¹⁰³. For the S1 subsite, replacing pyridine with isoquinoline produced a remarkable increase in potency (**60**, IC₅₀ = 0.72 $\mu\text{mol/L}$). The

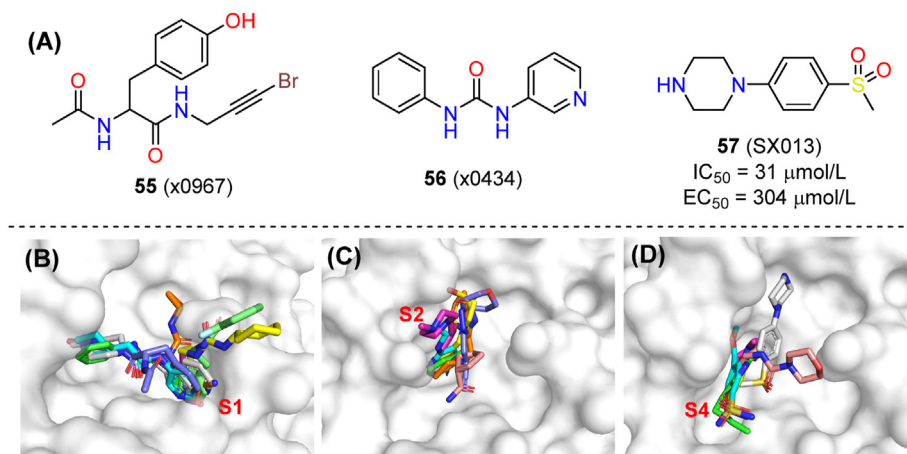


Figure 18 Fragment-based screening and optimization of SARS-CoV-2 M^{pro} inhibitors. (A) Chemical structures of **55** (x0967), **56** (x0434) and **57** (SX013) and biological activities of **57**. Superpositions of fragments occupying subsites S1, S2 and S4 subsites are shown in panels (B), (C) and (D), respectively.

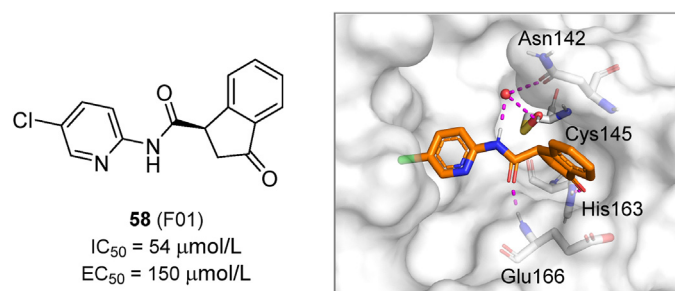


Figure 19 Chemical structure, biological activity and crystal structure of compound **58** in complex with SARS-CoV-2 M^{pro} (PDB ID: 7P51). Hydrogen bonds are shown as magenta dashed lines.

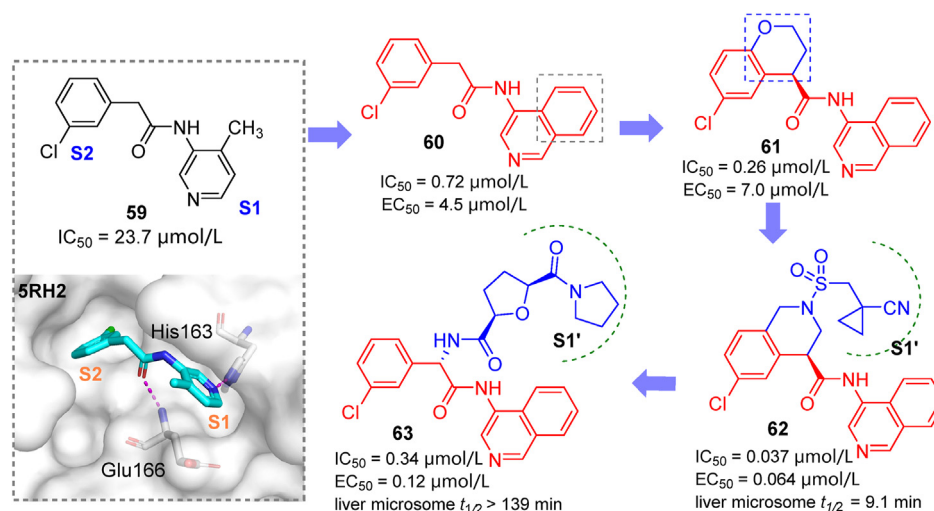


Figure 20 Derivatives (**60–63**) identified through lead discovery based on an aminoisoquinoline fragment **59**.

introduction of a chromane ring in S2 and its further replacement by a tetrahydroisoquinoline moiety concomitant with *N*-functionalization rendered compounds **61** and **62**, respectively. Compound **62** was found to be rather potent ($IC_{50} = 0.037 \mu\text{mol/L}$; $EC_{50} = 0.064 \mu\text{mol/L}$). Furthermore, using hundreds of crystal structures of M^{Pro} bound to different ligands, a computational model was trained to predict and rank novel M^{Pro} inhibitors¹⁰⁴. From synthetically-accessible virtual libraries, 40 analogs were identified by the algorithm and synthesized. The most promising compound **63** ($IC_{50} = 0.34 \mu\text{mol/L}$, $EC_{50(\text{Vero E6 cells})} = 0.12 \mu\text{mol/L}$), with an additional S1' binding group attached to main scaffold, had slightly weaker activity compared to **62**, but was characterized with high metabolic stability and low plasma binding. The large accommodation space in the S2/S1' subsites allowed researchers to conduct next-step derivatizations of aminoisoquinoline analogs assisted by the ranking model described above.

The structures and activities of fragments/hits in COVID-19 moonshot submission (represented by compound **64**) were collected to produce a ranking framework (Fig. 21A)¹⁰⁵. Instead of predicting accurate values of any compounds, this model could compare the estimated activity of two given compounds with high accuracy. From a library generated by adjusting substituents on training set compounds, three new inhibitors were identified, among which compound **65** showed the most potent activity (Fig. 21B). The ranking model could be a helpful aid in future screening of fragments targeting M^{Pro}.

The fragment library with co-crystal structures and the online COVID-19 Moonshot project provided great inspiration for the

discovery of novel non-covalent M^{Pro} inhibitors. In the future, more active compounds could be identified through the on-line crowdsourcing platform¹⁰⁶. FBDD possesses great potential in identifying lead compounds targeting M^{Pro}. Available fragment libraries can be enriched by computer-based screening with minimum cost and in a shorter period¹⁰⁷, while the critical evolution from fragments to leads requires greater efforts of medicinal chemists.

3.5. Discovering non-covalent M^{Pro} inhibitors using other strategies

3.5.1. Targeting M^{Pro} by exploiting natural products

Natural compounds had been a rich source of antiviral agents, both in ancient medicine and modern medicinal chemistry. Shikonin (**66**, Fig. 22A) was identified in HTS studies, inhibiting SARS-CoV-2 M^{Pro} with an IC_{50} value of $15.75 \mu\text{mol/L}$ ⁶⁹. Co-crystal studies confirmed its non-covalent binding mode (Fig. 22B)¹⁰⁸. However, the observed cytotoxicity of shikonin precluded further antiviral characterization and development. Based on a traditional Chinese medicine formulae for treating viral infections, baicalein (**67**) was identified as a potent M^{Pro} inhibitor in enzymatic assay and in phenotypic assay using Vero E6 cells¹⁰⁹. Multiple non-covalent interactions between baicalein and M^{Pro} were revealed by crystallographic studies (Fig. 22C).

Quercetin (**68**) was reported to target M^{Pro} with modest affinity¹¹⁰. Considering that selenium-functionalized natural compounds are known to exhibit different biological activities, aryl organoselenium groups were selectively introduced onto the C8

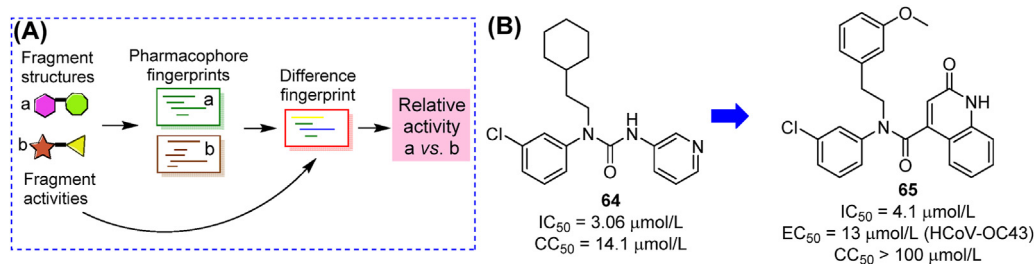


Figure 21 Schematic diagram and outcome of the ranking model driven by COVID-19 moonshot fragments. (A) Activity ranking based on pharmacophore fingerprints of two compounds; (B) Structures and activities of top training model compound **64** and predicted compound **65**.

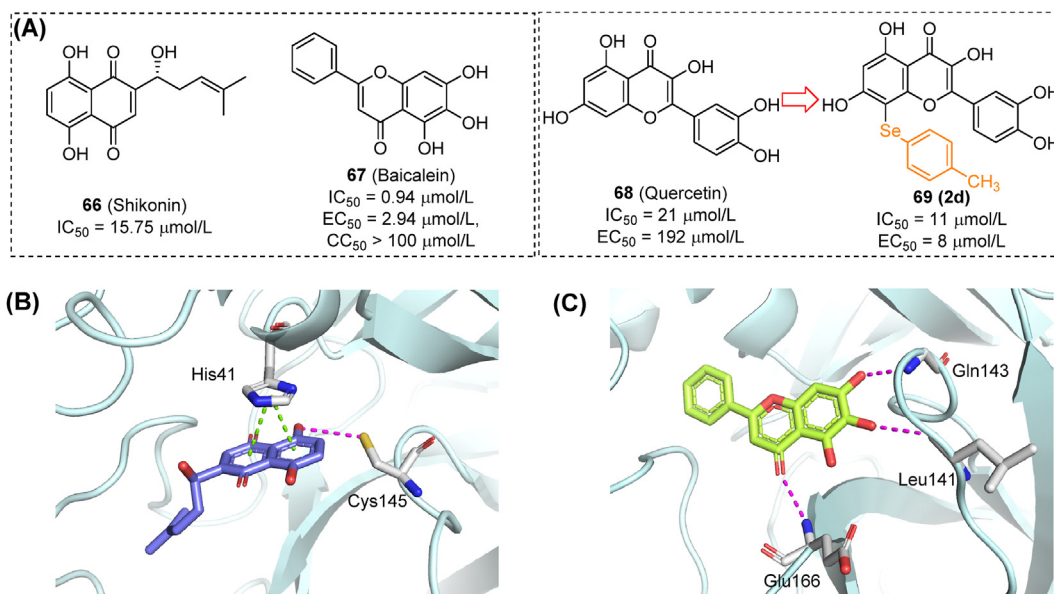


Figure 22 (A) Chemical structures and biological activities of the discussed natural products (**66–69**) targeting M^{pro} ; (B) Co-crystal structure of shikonin and M^{pro} (PDB ID: 7CA8); (C) Co-crystal structure of baicalein and M^{pro} (PDB ID: 6M2N). H-bonds are shown in magenta dashed lines. π – π stacking interactions are shown in green dashed lines.

position of the quercetin scaffold. The obtained compound **69 (2d)** showed significantly increased inhibitory activity in enzymatic assay ($IC_{50} = 11 \mu\text{mol/L}$) and antiviral activity in Vero cells ($EC_{50} = 8 \mu\text{mol/L}$, Fig. 22A)¹¹¹. However, for most natural products identified in bioactivity screening assays, the frequent occurrence of PAINS scaffolds¹¹² and a lack of drug-like properties of those compounds limit their further development towards clinical studies. Improved HTS methods and proper structural modifications are expected to provide suitable solutions to these caveats. In this scenario, the membrane permeability and pharmacokinetic properties of polyphenolic compounds should receive more attention, since prodrug derivatizations are frequently used for modifying phenolic hydroxyl structures.

3.5.2. Targeting M^{pro} by metal ions and complexes

Zinc ions (Zn^{2+}) play critical roles in biochemical reactions and protein structure. Previous research suggested that Zn^{2+} could inhibit SARS-CoV-1 by targeting M^{pro} ¹¹³. Several zinc salts (**70–73**, Fig. 23A) showed inhibitory activity against SARS-CoV-2 in the sub-micromolar range. Thus, zinc chloride (**70**) showed 50% and 100% inhibition at concentrations of 0.399 and 6.25 $\mu\text{mol/L}$, respectively. However, this inhibition was reversible in the presence of high concentrations of substrate or EDTA. Co-crystallization studies confirmed that Zn^{2+} impairs M^{pro} function by chelating with the side chains of His41 and Cys145 and interacting at the S1' subsite (Fig. 23B, PDB ID: 7DK1)¹¹⁴. Based on this finding, the metal ion promoter hinokitol (**74**, β -thujaplicin) was used to

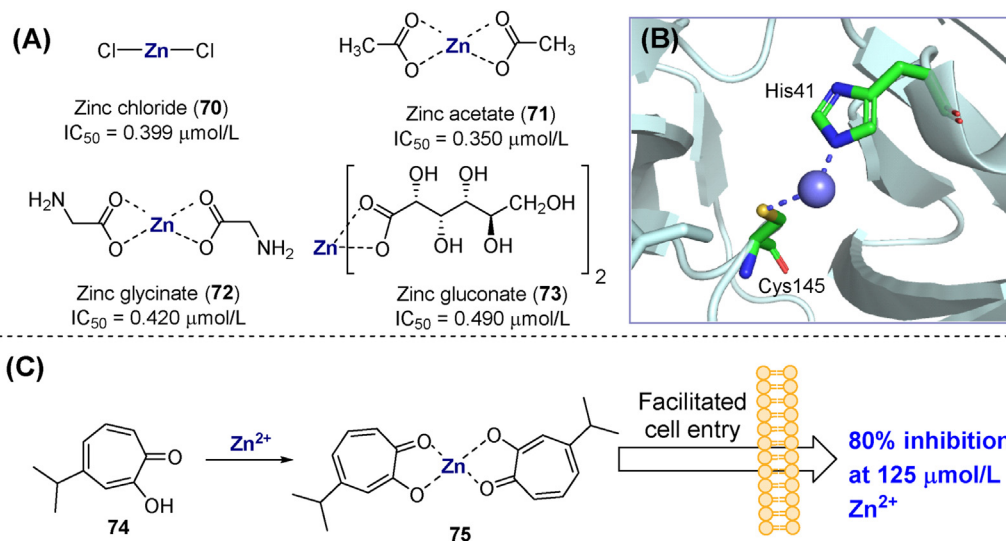


Figure 23 Metal complexes targeting M^{pro} . (A) Chemical structures and biological activities of zinc salts/coordinates inhibiting SARS-CoV-2 M^{pro} . (B) Crystal structure of zinc ion bound to the M^{pro} catalytic site (PDB ID: 7DK1). (C) Chemical structures and activity of zinc–hinokitol complexes.

increase the zinc concentration in the cytoplasm. The results showed that 125 $\mu\text{mol/L}$ Zn^{2+} and 30 $\mu\text{mol/L}$ compound **75** inhibited 80% virus infection in Vero E6 cells without significant toxicity (Fig. 23C)¹¹⁵. Despite these findings, the antiviral potency and safety profile of metal-based M^{pro} inhibitors are not good enough to turn them into therapeutic agents.

3.5.3. Targeting M^{pro} by non-covalent binding of peptides

Peptide-like covalent inhibitors play a significant role in antiviral research. However, a few non-covalent cyclic peptide M^{pro} inhibitors have been reported as well. Screening over a mRNA/cDNA-encoded peptide library using an immobilized M^{pro} led to the identification of compounds **76** (peptide 1) and **77** (peptide 6)

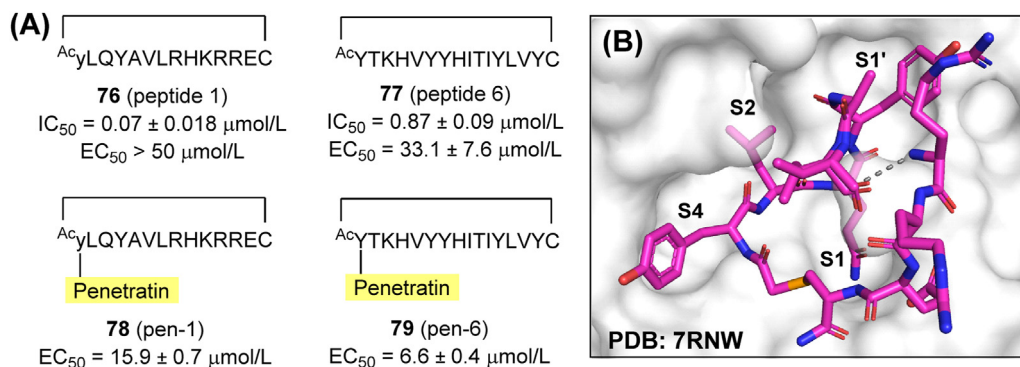


Figure 24 Peptides as non-covalent inhibitors of SARS-CoV-2 M^{pro}. (A) Amino acid sequences and biological activities of peptides **76**–**79**. (B) Co-crystal structure of **76** in complex with M^{pro} (PDB ID: 7RNW). The gray dashed line represents undetermined atoms.

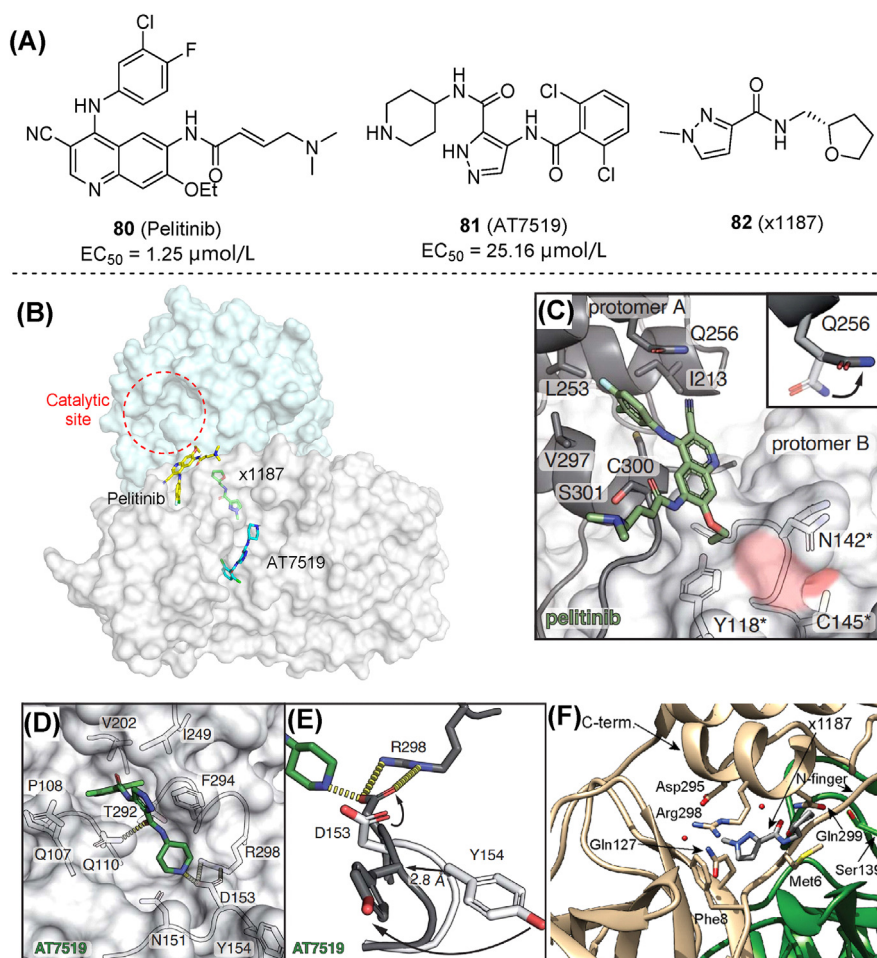


Figure 25 Small molecules targeting non-catalytic sites. (A, B) Chemical structures, activities, and binding sites of **80** (pelitinib), **81** (AT7519) and **82** (x1187). (C) Co-crystal structures of pelitinib bound at the M^{pro} dimer surface (PDB ID: 7AXM). (D) Ligand interactions of **81** with M^{pro} (PDB ID: 7AGA). (E) Conformational changes of Arg298 and Tyr154 in the **81**-bound M^{pro} structure (black) compared with apo-M^{pro} (light gray). (F) Co-crystal structure of **82** bound at the M^{pro} dimer surface (PDB ID: 5RFA)^{118,119}.

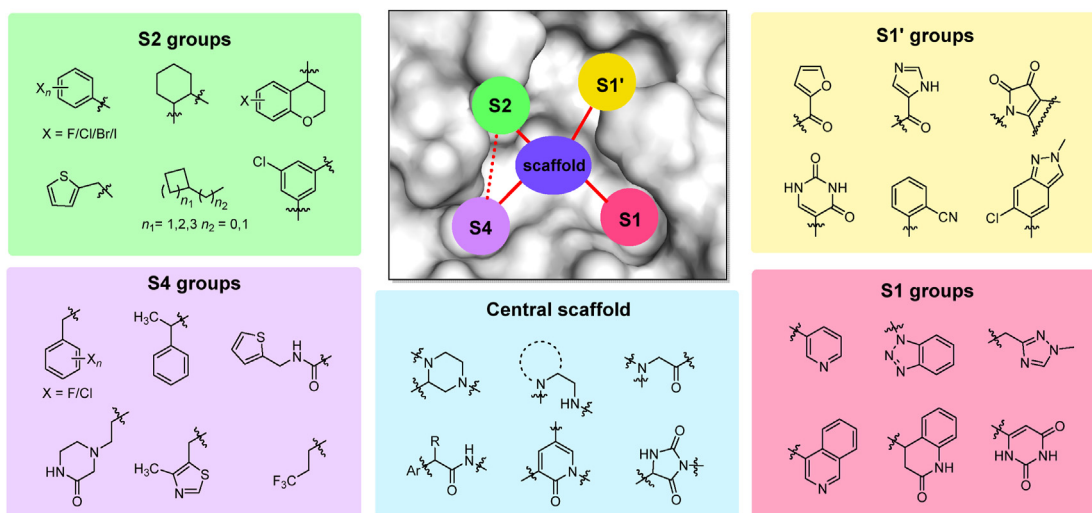


Figure 26 Overview of key pharmacophores and privileged groups in non-covalent M^{pro} inhibitors.

(Fig. 24A). Both of them showed low IC_{50} values (0.07 and 0.87 $\mu\text{mol/L}$, respectively) and high selectivity towards host targets, while their concentration was stably maintained in human plasma¹¹⁶. However, in cell-based antiviral assays, the most potent inhibitor (**76**) had no activity up to a concentration of 50 $\mu\text{mol/L}$. To address this problem, penetratin, a 16-amino acid peptide promoting cell entry, was conjugated to the C-terminal of **76** and **77** to obtain compounds **78** (pen-1) and **79** (pen-6). The two modified peptides displayed enhanced antiviral activity as intended (Fig. 24A). The co-crystal structure of a selenoether analog of **76** with M^{pro} revealed its interaction mode with the active site and even the dimer surface (Fig. 24B). Despite showing high potency, previously reported non-covalent peptide M^{pro} inhibitors may have limited bioavailability and poor metabolic stability.

3.5.4. Targeting non-catalytic sites of SARS-CoV-2 M^{pro}

Non-catalytic sites of M^{pro} refer to potential allosteric sites and binding positions on the dimer surface, which may accommodate small molecules and thus disrupt enzymatic function¹¹⁷. Two allosteric sites of M^{pro} were revealed by co-crystallization studies with small molecules¹¹⁸. The first site is at the C-terminal dimerization domain and was targeted by five molecules in a screening study. Among them, **80** (pelininib, Fig. 25A and B) exhibited the most potent antiviral activity ($EC_{50} = 1.25 \mu\text{mol/L}$). Pelininib shows hydrophobic interactions with terminal amino acid residues in a key pocket, whose integrity is critical for enzymatic activity (Fig. 25C). Molecules binding to this site may directly disrupt dimer stability. The second site is a groove between domains II and III, occupied by **81** (AT7519). The amino group from piperidine ring of **81** facilitated the displacement of Asp153, enabling it to form a new salt bridge with the side chain of Arg298 (Fig. 25D and E). As mutations or disruptions of Arg298 were known to destabilize dimerization and affect the active site, this fact explains the inhibition mechanism of **81**. Follow-up studies developed a native mass spectrometry assay, confirming that fragment **82** (x1187) interacts with the dimerization interface and promoted M^{pro} dissociation¹¹⁹. Co-crystal structures of M^{pro} complexed with **82** showed that this molecule is also approximate to Arg298, but located at a slightly different position compared with **81** (Fig. 25F). The mechanism of action of M^{pro} allosteric inhibitors needs to be understood, before serving as a guide for designing new compounds.

There is no doubt that advances in discovering allosteric M^{pro} inhibitors provide an alternative path for the discovery of non-covalent inhibitors, although more detailed binding analyses and SAR studies are needed to improve their potential capabilities. Moreover, drug design strategies targeting allosteric sites have been widely applied to HIV reverse transcriptases, integrases, and herpes simplex viruses¹²⁰. Allosteric sites have several advantages over active site binders^{121–123}: (i) all allosteric inhibitors identified so far have reversible effects, making them safer than many covalent M^{pro} inhibitors previously discovered^{124,125}; (ii) inhibitors targeting allosteric sites could help to overcome the effects of drug resistance-associated mutations appearing in the active site of the enzyme¹¹⁷. Therefore, the M^{pro} allosteric sites might be another promising start for the discovery of broad-spectrum anti-coronavirus agents that can act alone or in combination with the other competitive M^{pro} inhibitors.

How to verify that specific compounds act on allosteric sites rather than the catalytic site also requires special attention. As complements to X-ray crystallography, we believe that changes in the relative amounts of monomeric and dimeric M^{pro} could also be measured in biochemical assays, such as native polyacrylamide gel electrophoresis, size exclusion chromatography, or native mass spectrometry.

4. Conclusions, challenges and future directions

Although the search for non-covalent SARS-CoV-2 M^{pro} inhibitors had just started, remarkable achievements and future contributions in the battle against COVID-19 cannot be ignored. To date, it is becoming clearer that non-covalent M^{pro} inhibitors have a larger space for optimization, and are more likely to develop into potential oral agents with lower clinical risks. Positive outcomes from clinical trials of ensitrelvir (S-217622) and future candidates will also boost the rising interest in this field, which will act as an indispensable counterpart of traditional covalent peptidomimetics. From this perspective, we summarized the development concepts, strategies and methods under the whole course of non-covalent M^{pro} inhibitors discovery, from primitive hits to pre-clinical evaluations. Various strategies have shown strong interconnections and are valuable references for future developments in this field. We aim to provide a reliable source of information for this emerging field of anti-SARS-CoV-2 drug

discovery, aiming to explore prospective non-covalent M^{pro} inhibitors with diverse structures and prominent antiviral potency comparable with approved therapeutics.

4.1. Progress and challenge in developing non-covalent M^{pro} inhibitors

Most of the compounds discussed above share similar scaffolds and pharmacophores in each subsite, despite being identified through different strategies. The most representative privileged fragments among existing non-covalent SARS-CoV-2 M^{pro} inhibitors are summarized in Fig. 26. Important features of the inhibitor binding site include the lipophilic pockets S2 and S4, where His41, Gln189 and Glu166 are critical components. While the key amino acids of S1 and S1' are His163, Gly143, Cys145 and Thr26. These structural constraints facilitate the molecular hybridization strategy in the discovery of non-covalent M^{pro} inhibitors. The application of advanced computational methods (such as pharmacophore-linked fragment virtual screening, or auto core fragment *in silico* screening)^{126,127} in the assembly of pharmacophore fragments at each subsite with optimizable scaffolds may also contribute to the rational design of M^{pro} inhibitors.

Although some seemingly good non-covalent M^{pro} inhibitors have been reported, there is still a long way ahead for many non-covalent M^{pro} inhibitors to advance into clinical trials and eventually approval. Several major barriers need to be solved in this effort. First, the inhibitory activity of most of the non-covalent inhibitors is significantly weaker than that of peptide-like covalent inhibitors. Second, there is a need for structurally diverse inhibitors. The scaffolds of current M^{pro} inhibitors usually derive from previous SARS-CoV-1 inhibitors, thereby requiring further exploration of disparate new scaffolds with better occupation of the M^{pro} active site. Third, unfavorable DMPK properties and high toxicity is a common weakness of most summarized compounds, which limit the development of M^{pro} inhibitors^{86,92}. Thus, PK profiles should be considered in structural optimization. Fourth, advanced computer screening technologies have not been effectively combined with experimental practice.

4.2. Improvement of current strategies

On the solid foundation of previous studies, there are several necessary complements and improvements to current strategies. First, multiple parameters of candidate compounds should be considered simultaneously in optimization¹²⁸. Encouraging progress in the determination of activity profiles has been already attained, but this was not the endpoint of rational optimization. Besides inhibitory activity, compound druggability including solubility, metabolic stability, hERG toxicity and potential side effects should also be addressed.

Second, accurate and efficient screening methods are still needed to provide hit compounds for future modification. Discovery of ensitrelvir highlights the importance of efficient virtual screening and rational follow-up modification. As alternatives to the classical HTS paradigm, miniaturized high-throughput synthesis (including DNA-encoding and click-chemistry-based combinatorial libraries)^{129–131} and high-throughput protein crystallography (X-ray crystallographic screening)^{132–134} can accelerate the early steps of M^{pro}-targeted drug discovery.

Third, ligand efficacy should receive further attention in the optimization of M^{pro} hit compounds. Although extended pocket occupation may lead to higher activity, ligand efficacy may be

reduced if bulkier molecules are involved in these developments. In contrast, “magic” groups such as single CH₃ or Cl which allow a high gain in potency^{135,136}, are expected to improve ligand efficacy of current lead compounds.

Finally, developing inhibitors targeting non-catalytic sites based on the crystal structure could be successful alternatives. For targeting the dimer interface of M^{pro}, inhibitors should be able to disrupt critical protein–protein interactions while maintaining high affinity for relatively large structures, as demonstrated for well-characterized inhibitors of HIV-1 capsid¹³⁷. Rational design and SAR studies of M^{pro} allosteric inhibitors are required.

4.3. Moving on to the “second phase” in the discovery of M^{pro} inhibitors

The emerging and transmission of coronavirus over past decades reminded us of the necessity to develop and stock effective antiviral drugs while getting ready to combat next waves of SARS-CoV-2 pandemic or future coronavirus breaks. A turning point in race has been reached. In the past “first phase”, we have accumulated hit compounds, assay systems and crystal structures for non-covalent M^{pro} inhibitor development. From the beginning of the second phase, effective, oral-available, and M^{pro} inhibitors active against drug-resistant strains are greatly needed. Among the clinically dominant SARS-CoV-2 strains, resistance towards M^{pro} inhibitors is rare. However, a broad use of nirmatrelvir and ensitrelvir will likely select resistant strains. To prevent future epidemics caused by drug-resistant strains, principles based on the substrate envelope^{138,139} hypotheses could be applied. From the defined M^{pro} substrate envelope, researchers could find a balance between high activity and resilience, identifying next-generation drug candidates^{140–142}. Other prevailing strategies, including macrocyclization, multivalent ligands and targeted protein degradation (PROTAC, molecular glues and hydrophobic tags) also have great potential^{143–148}.

In summary, we hope this comprehensive analysis will provide a novel perspective on drug discovery approaches currently targeting SARS-CoV-2 M^{pro}. Retrospective and critical analysis of established strategies, accompanied by the exploration of novel scaffolds, would effectively boost the identification of potent M^{pro} inhibitors with an expected clinical impact in the future.

Acknowledgments

We gratefully acknowledge financial support from Major Basic Research Project of Shandong Provincial Natural Science Foundation (ZR2021ZD17, China), Science Foundation for Outstanding Young Scholars of Shandong Province (ZR2020JQ31, China), Foreign Cultural and Educational Experts Project (GXL20200015001, China), Guangdong Basic and Applied Basic Research Foundation (2021A1515110740, China), China Postdoctoral Science Foundation (2021M702003). This work was supported in part by the Ministry of Science and Innovation of Spain through grant PID2019-104176RB-I00/AEI/10.13039/501100011033 awarded to Luis Menéndez-Arias; An institutional grant of the Fundación Ramón Areces (Madrid, Spain) to the CBMSO is also acknowledged. Luis Menéndez-Arias is member of the Global Virus Network.

Author contributions

Letian Song and Shenghua Gao contributed equally to this work. Letian Song and Shenghua Gao drafted the manuscript; Bing Ye,

Mianling Yang and Yusen Cheng drew figures of the manuscript; Dongwei Kang, Fan Yi, Jin-Peng Sun, Luis Menéndez-Arias and Johan Neyts revised and checked the manuscript. Peng Zhan and Xinyong Liu polished the manuscript and supervised the project. All authors read and approved the final manuscript.

Conflicts of interest

The authors declare no competing financial interest.

References

- Zhou P, Yang XL, Wang XG, Hu B, Zhang L, Zhang W, et al. A pneumonia outbreak associated with a new coronavirus of probable bat origin. *Nature* 2020;**579**:270–3.
- Hu B, Guo H, Zhou P, Shi ZL. Characteristics of SARS-CoV-2 and COVID-19. *Nat Rev Microbiol* 2021;**19**:141–54.
- World Health Organization. WHO coronavirus (COVID-19) dashboard. Available from: <https://covid19.who.int/>.
- Choi JY, Smith DM. SARS-CoV-2 variants of concern. *Yonsei Med J* 2021;**62**:961–8.
- Cameroni E, Bowen JE, Rosen LE, Saliba C, Zepeda SK, Culap K, et al. Broadly neutralizing antibodies overcome SARS-CoV-2 Omicron antigenic shift. *Nature* 2022;**602**:664–70.
- Feikin DR, Higdon MM, Abu-Raddad LJ, Andrews N, Araos R, Goldberg Y, et al. Duration of effectiveness of vaccines against SARS-CoV-2 infection and covid-19 disease: results of a systematic review and meta-regression. *Lancet* 2022;**399**:924–44.
- Chen J, Wang R, Gilby NB, Wei GW. Omicron variant (B.1.1.529): infectivity, vaccine breakthrough, and antibody resistance. *J Chem Inf Model* 2022;**62**:412–22.
- Agost-Beltrán L, de la Hoz-Rodríguez S, Bou-Iserte L, Rodríguez S, Fernández-de-la-Pradilla A, González FV. Advances in the development of SARS-CoV-2 Mpro inhibitors. *Molecules* 2022;**27**:2523.
- Tian L, Qiang T, Liang C, Ren X, Jia M, Zhang J, et al. RNA-dependent RNA polymerase (RdRp) inhibitors: the current landscape and repurposing for the COVID-19 pandemic. *Eur J Med Chem* 2021;**213**:113201.
- Tian L, Pang Z, Li M, Lou F, An X, Zhu S, et al. Molnupiravir and its antiviral activity against COVID-19. *Front Immunol* 2022;**4**:855496.
- Pilkington V, Pepperrell T, Hill A. A review of the safety of favipiravir—a potential treatment in the COVID-19 pandemic?. *J Virus Erad* 2020;**6**:45–51.
- Good SS, Westover J, Jung KH, Zhou XJ, Moussa A, La Colla P, et al. AT-527, a double prodrug of a guanosine nucleotide analog, is a potent inhibitor of SARS-CoV-2 *in vitro* and a promising oral antiviral for treatment of COVID-19. *Antimicrob Agents Chemother* 2021;**65**. 024799–20.
- Wang Y, Zhang D, Du G, Du R, Zhao J, Jin Y, et al. Remdesivir in adults with severe COVID-19: a randomised, double-blind, placebo-controlled, multicentre trial. *Lancet* 2020;**395**:1569–78.
- Gao S, Huang T, Song L, Xu S, Cheng Y, Cherukupalli S, et al. Medicinal chemistry strategies towards the development of effective SARS-CoV-2 inhibitors. *Acta Pharm Sin B* 2022;**12**:581–99.
- Clinical trials arena. Atea's AT-527 fails to meet primary goal of Phase II Covid-19 trial. Available from: <https://www.clinicaltrialsarena.com/news/atea-at-527-primary-goal/>.
- Eloy P, Le Grand R, Malvy D, Guedj J. Combined treatment of molnupiravir and favipiravir against SARS-CoV-2 infection: one + zero equals two?. *EBioMedicine* 2021;**74**:103663.
- Hashemian SMR, Pourhanifeh MH, Hamblin MR, Shahrzad MK, Mirzaei H. RdRp inhibitors and COVID-19: is molnupiravir a good option?. *Biomed Pharmacother* 2022;**146**:112517.
- Drożdżal S, Rosik J, Lechowicz K, Machaj F, Szostak B, Przybyciński J, et al. An update on drugs with therapeutic potential for SARS-CoV-2 (COVID-19) treatment. *Drug Resist Updates* 2021;**59**:100794.
- Cui W, Yang K, Yang H. Recent progress in the drug development targeting SARS-CoV-2 main protease as treatment for COVID-19. *Front Mol Biosci* 2020;**7**:616341.
- Simcere. XIANNUOXIN is put into production and launched today, contributing to China's economic development and the public's health. Available from: <http://en.simcere.com/news/detail.aspx?mtt=328..>
- Chen X, Wang J, Huang J, Liu Z, Long C, Chen S, et al. *Keto-amide derivative and application thereof in treatment of coronavirus infection*. 2023. CN 115594734 A.
- Shionogi. Xocova® (ensitrelvir fumaric acid) tablets 125 mg approved in Japan for the treatment of SARS-CoV-2 infection, under the emergency regulatory approval system. Available from: <https://www.shionogi.com/us/en/news/2022/11/xocova-ensitrelvir-fumaric-acid-tablets-125mg-approved-in-japan-for-the-treatment-of-sars-cov-2-infection,-under-the-emergency-regulatory-approval-system.html>.
- Pang X, Xu W, Liu Y, Li H, Chen L. The research progress of SARS-CoV-2 main protease inhibitors from 2020 to 2022. *Eur J Med Chem* 2023;**257**:115491.
- Macip G, Garcia-Segura P, Mestres-Truyol J, Saldivar-Espinoza B, Pujadas G, Garcia-Vallvé S. A review of the current landscape of SARS-CoV-2 main protease inhibitors: have we hit the bullseye yet? *Int J Mol Sci* 2021;**23**:259.
- Citarella A, Scala A, Piperno A, Micale N. SARS-CoV-2 M^{pro}: a potential target for peptidomimetics and small-molecule inhibitors. *Biomolecules* 2021;**11**:607.
- Rahimi A, Mirzazadeh A, Tavakolpour S. Genetics and genomics of SARS-CoV-2: a review of the literature with the special focus on genetic diversity and SARS-CoV-2 genome detection. *Genomics* 2021;**113**(1 Pt 2):1221–32.
- Fehr AR, Perlman S. Coronaviruses: an overview of their replication and pathogenesis. *Methods Mol Biol* 2015;**1282**:1–23.
- Shin D, Mukherjee R, Grewe D, Bojkova D, Baek K, Bhattacharya A, et al. Papain-like protease regulates SARS-CoV-2 viral spread and innate immunity. *Nature* 2020;**587**:657–62.
- Kirtipal N, Bharadwaj S, Kang SG. From SARS to SARS-CoV-2, insights on structure, pathogenicity and immunity aspects of pandemic human coronaviruses. *Infect Genet Evol* 2020;**85**:104502.
- Rawlings ND, Barrett AJ, Thomas PD, Huang X, Bateman A, Finn RD. The MEROPS database of proteolytic enzymes, their substrates and inhibitors in 2017 and a comparison with peptidases in the PANTHER database. *Nucleic Acids Res* 2018;**46**:D624–32.
- Bafna K, Cioffi CL, Krug RM, Montelione GT. Structural similarities between SARS-CoV2 3CL^{pro} and other viral proteases suggest potential lead molecules for developing broad spectrum antivirals. *Front Chem* 2022;**10**:948553.
- Melo-Filho CC, Bobrowski T, Martin HJ, Sessions Z, Popov KI, Moorman NJ, et al. Conserved coronavirus proteins as targets of broad-spectrum antivirals. *Antivir Res* 2022;**204**:105360.
- Sabbah DA, Hajjo R, Bardaweel SK, Zhong HA. An updated review on SARS-CoV-2 main proteinase (Mpro): protein structure and small-molecule inhibitors. *Curr Top Med Chem* 2021;**21**:442–60.
- Kneller DW, Phillips G, Weiss KL, Pant S, Zhang Q, O'Neill HM, et al. Unusual zwitterionic catalytic site of SARS-CoV-2 main protease revealed by neutron crystallography. *J Biol Chem* 2020;**295**:17365–73.
- Banerjee R, Perera L, Tillekeratne LMV. Potential SARS-CoV-2 main protease inhibitors. *Drug Discov Today* 2021;**26**:804–16.
- Arya R, Kumari S, Pandey B, Mistry H, Bihani SC, Das A, et al. Structural insights into SARS-CoV-2 proteins. *J Mol Biol* 2021;**433**:166725.
- Zhao Y, Zhu Y, Liu X, Jin Z, Duan Y, Zhang Q, et al. Structural basis for replicase polyprotein cleavage and substrate specificity of main

- protease from SARS-CoV-2. *Proc Natl Acad Sci U S A* 2022;**119**: e2117142119.
38. Sepay N, Saha PC, Shahzadi Z, Chakraborty A, Halder UC. A crystallography-based investigation of weak interactions for drug design against COVID-19. *Phys Chem Chem Phys* 2021;**23**:7261–70.
 39. Shitrit A, Zaidman D, Kalid O, Bloch I, Doron D, Yarnizky T, et al. Conserved interactions required for inhibition of the main protease of severe acute respiratory syndrome coronavirus 2 (SARS-CoV-2). *Sci Rep* 2020;**10**:20808.
 40. Said MA, Albohy A, Abdelrahman MA, Ibrahim HS. Importance of glutamine 189 flexibility in SARS-CoV-2 main protease: lesson learned from *in silico* virtual screening of ChEMBL database and molecular dynamics. *Eur J Pharmaceut Sci* 2021;**160**:105744.
 41. Ábrányi-Balogh P, Petri L, Imre T, Szijj P, Scarpino A, Hrust M, et al. A road map for prioritizing warheads for cysteine targeting covalent inhibitors. *Eur J Med Chem* 2018;**160**:94–107.
 42. Pillaiyar T, Flury P, Krüger N, Su H, Schäkel L, Barbosa Da Silva E, et al. Small-molecule thioesters as SARS-CoV-2 main protease inhibitors: enzyme inhibition, structure–activity relationships, antiviral activity, and X-ray structure determination. *J Med Chem* 2022;**65**: 9376–95.
 43. Ma XR, Alugubelli YR, Ma Y, Vatansever EC, Scott DA, Qiao Y, et al. MPI8 is potent against SARS-CoV-2 by inhibiting dually and delectively the SARS-CoV-2 main protease and the host Cathepsin L. *ChemMedChem* 2022;**17**:e202100456.
 44. Iketani S, Mohri H, Culbertson B, Hong SJ, Duan Y, Luck MI, et al. Multiple pathways for SARS-CoV-2 resistance to nirmatrelvir. *Nature* 2023;**613**:558–64.
 45. de Oliveira VM, Ibrahim MF, Sun X, Hilgenfeld R, Shen J. H172Y mutation perturbs the S1 pocket and nirmatrelvir binding of SARS-CoV-2 main protease through a nonnative hydrogen bond. *Research square* 2022. Available from: <https://doi.org/10.21203/rs.3.rs-1915291/v1>.
 46. Hilgenfeld R. From SARS to MERS: crystallographic studies on coronaviral proteases enable antiviral drug design. *FEBS J* 2014;**281**: 4085–96.
 47. Goyal B, Goyal D. Targeting the dimerization of the main protease of coronaviruses: a potential broad-spectrum therapeutic strategy. *ACS Comb Sci* 2020;**22**:297–305.
 48. Pekel H, Ilter M, Sensoy O. Inhibition of SARS-CoV-2 main protease: a repurposing study that targets the dimer interface of the protein. *J Biomol Struct Dyn* 2021;**13**:1–16.
 49. Nashed NT, Aniana A, Ghirlando R, Chiliveri SC, Louis JM. Modulation of the monomer-dimer equilibrium and catalytic activity of SARS-CoV-2 main protease by a transition-state analog inhibitor. *Commun Biol* 2022;**5**:160.
 50. Fornasier E, Macchia ML, Giachin G, Sosic A, Pavan M, Sturlese M, et al. A new inactive conformation of SARS-CoV-2 main protease. *Acta Crystallogr D Struct Biol* 2022;**78**(Pt 3):363–78.
 51. Santos LH, Kronenberger T, Almeida RG, Silva EB, Rocha REO, Oliveira JC, et al. Structure-based identification of naphthoquinones and derivatives as novel inhibitors of main protease M^{pro} and papain-like protease PL^{pro} of SARS-CoV-2. *J Chem Inf Model* 2022;**62**: 6553–73.
 52. Lee JY, Kuo CJ, Shin JS, Jung E, Liang PH, Jung YS. Identification of non-covalent 3C-like protease inhibitors against severe acute respiratory syndrome coronavirus-2 via virtual screening of a Korean compound library. *Bioorg Med Chem Lett* 2021;**42**:128067.
 53. Zhai T, Zhang F, Haider S, Kraut D, Huang Z. An integrated computational and experimental approach to identifying inhibitors for SARS-CoV-2 3CL protease. *Front Mol Biosci* 2021;**8**:661424.
 54. Mercorelli B, Desantis J, Celegato M, Bazzacco A, Siragusa L, Benedetti P, et al. Discovery of novel SARS-CoV-2 inhibitors targeting the main protease Mpro by virtual screenings and hit optimization. *Antivir Res* 2022;**204**:105350.
 55. Abo Elmaaty A, Eldehna WM, Khattab M, Kutkat O, Alnajjar R, El-Taweel AN, et al. Anticoagulants as potential SARS-CoV-2 M^{pro} inhibitors for COVID-19 patients: *in vitro*, molecular docking, molecular dynamics, DFT, and SAR studies. *Int J Mol Sci* 2022;**23**: 12235.
 56. Vatansever EC, Yang KS, Drelich AK, Kratch KC, Cho CC, Kempaiah KR, et al. Bepridil is potent against SARS-CoV-2 *in vitro*. *Proc Natl Acad Sci U S A* 2021;**18**:e2012201118.
 57. Luttens A, Gullberg H, Abdurakhmanov E, Vo DD, Akaberi D, Talibov VO, et al. Ultralarge virtual screening identifies SARS-CoV-2 main protease inhibitors with broad-spectrum activity against coronaviruses. *J Am Chem Soc* 2022;**144**:2905–20.
 58. Gorgulla C, Padmanabha Das KM, Leigh KE, Cesugli M, Fischer PD, Wang ZF, et al. A multi-pronged approach targeting SARS-CoV-2 proteins using ultra-large virtual screening. *iScience* 2021;**24**:102021.
 59. Rossetti GG, Ossorio MA, Rempel S, Kratzel A, Dionellis VS, Barriot S, et al. Non-covalent SARS-CoV-2 M^{pro} inhibitors developed from *in silico* screen hits. *Sci Rep* 2022;**12**:2505.
 60. Clyde A, Galanie S, Kneller DW, Ma H, Babuji Y, Blaiszik B, et al. High-throughput virtual screening and validation of a SARS-CoV-2 main protease noncovalent inhibitor. *J Chem Inf Model* 2022;**62**: 116–28.
 61. Kneller DW, Li H, Galanie S, Phillips G, Labbé A, Weiss KL, et al. Structural, electronic, and electrostatic determinants for inhibitor binding to subsites S1 and S2 in SARS-CoV-2 main protease. *J Med Chem* 2021;**64**:17366–83.
 62. Xu T, Xu M, Zhu W, Chen CZ, Zhang Q, Zheng W, et al. Efficient identification of anti-SARS-CoV-2 compounds using chemical structure- and biological activity-based modeling. *J Med Chem* 2022;**65**:4590–9.
 63. Gentile F, Fernandez M, Ban F, Ton AT, Mslati H, Perez CF, et al. Automated discovery of noncovalent inhibitors of SARS-CoV-2 main protease by consensus deep docking of 40 billion small molecules. *Chem Sci* 2021;**12**:15960–74.
 64. Li SG, Yang KS, Blankenship LR, Cho CD, Xu S, Wang H, et al. An enhanced hybrid screening approach to identify potent inhibitors for the SARS-CoV-2 main protease from the NCI compound library. *Front Chem* 2022;**10**:816576.
 65. Gimeno A, Ojeda-Montes MJ, Tomás-Hernández S, Cereto-Massagué A, Beltrán-Debón R, Mulero M, et al. The light and dark sides of virtual screening: what is there to know?. *Int J Mol Sci* 2019;**20**:1375.
 66. Macip G, Garcia-Segura P, Mestres-Truyol J, Saldívar-Espinoza B, Ojeda-Montes MJ, Gimeno A, et al. Haste makes waste: a critical review of docking-based virtual screening in drug repurposing for SARS-CoV-2 main protease (M-pro) inhibition. *Med Res Rev* 2022;**42**:744–69.
 67. Lyu J, Irwin JJ, Shoichet BK. Modeling the expansion of virtual screening libraries. *Nat Chem Biol* 2023;**19**:712–8.
 68. Ma C, Sacco MD, Hurst B, Townsend JA, Hu Y, Szeto T, et al. Boceprevir, GC-376, and calpain inhibitors II, XII inhibit SARS-CoV-2 viral replication by targeting the viral main protease. *Cell Res* 2020;**30**:678–92.
 69. Jin Z, Du X, Xu Y, Deng Y, Liu M, Zhao Y, et al. Structure of M^{pro} from SARS-CoV-2 and discovery of its inhibitors. *Nature* 2020;**582**: 289–93.
 70. Dražić T, Kühn N, Leuthold MM, Behnam MAM, Klein CD. Efficiency improvements and discovery of new substrates for a SARS-CoV-2 main protease FRET assay. *SLAS Discov* 2021;**26**: 1189–99.
 71. Tan H, Hu Y, Jadhav P, Tan B, Wang J. Progress and challenges in targeting the SARS-CoV-2 papain-like protease. *J Med Chem* 2022;**65**:7561–80.
 72. Brown AS, Ackerley DF, Calcott MJ. High-throughput screening for inhibitors of the SARS-CoV-2 protease using a FRET-biosensor. *Molecules* 2020;**25**:4666.
 73. Sondag D, Merx J, Rossing E, Boltje TJ, Löwik DWPM, Nelissen FHT, et al. Luminescent assay for the screening of SARS-CoV-2 M^{pro} inhibitors. *Chembiochem* 2022;**23**:e202200190.

74. Ma C, Tan H, Choza J, Wang Y, Wang J. Validation and invalidation of SARS-CoV-2 main protease inhibitors using the Flip-GFP and Protease-Glo luciferase assays. *Acta Pharm Sin B* 2022;**12**:1636–51.
75. Smith E, Davis-Gardner ME, Garcia-Ordóñez RD, Nguyen TT, Hull M, Chen E, et al. High throughput screening for drugs that inhibit 3C-like protease in SARS-CoV-2. *SLAS Discov* 2020;**25**:1152–61.
76. Zhu W, Xu M, Chen CZ, Guo H, Shen M, Hu X, et al. Identification of SARS-CoV-2 3CL protease inhibitors by a quantitative high-throughput screening. *ACS Pharmacol Transl Sci* 2020;**3**:1008–16.
77. Rothan HA, Teoh TC. Cell-based high-throughput screening protocol for discovering antiviral inhibitors against SARS-CoV-2 main protease (3CLpro). *Mol Biotechnol* 2021;**63**:240–8.
78. Drayman N, DeMarco JK, Jones KA, Azizi SA, Froggatt HM, Tan K, et al. Masitinib is a broad coronavirus 3CL inhibitor that blocks replication of SARS-CoV-2. *Science* 2021;**373**:931–6.
79. Hou N, Shuai L, Zhang L, Xie X, Tang K, Zhu Y, et al. Development of highly potent non-covalent inhibitors of SARS-CoV-2 3CLpro. *ACS Cent Sci* 2023;**9**:217–27.
80. Cui M, Nguyen D, Gaillez MP, Heiden S, Lin W, Thompson M, et al. Trio-pharmacophore DNA-encoded chemical library for simultaneous selection of fragments and linkers. *Nat Commun* 2023;**14**:1481.
81. Lockbaum GJ, Reyes AC, Lee JM, Tilvawala R, Nalivaika EA, Ali A, et al. Crystal structure of SARS-CoV-2 main protease in complex with the non-covalent inhibitor ML188. *Viruses* 2021;**13**:174.
82. Kitamura N, Sacco MD, Ma C, Hu Y, Townsend JA, Meng X, et al. Expedited approach toward the rational design of noncovalent SARS-CoV-2 main protease inhibitors. *J Med Chem* 2022;**65**:2848–65.
83. Quan BX, Shuai H, Xia AJ, Hou Y, Zeng R, Liu XL, et al. An orally available M^{Pro} inhibitor is effective against wild-type SARS-CoV-2 and variants including Omicron. *Nat Microbiol* 2022;**7**:716–25.
84. De Castro S, Stevaert A, Maldonado M, Delpal A, Vandeput J, Van Loy B, et al. A versatile class of 1,4,4-trisubstituted piperidines block coronavirus replication *in vitro*. *Pharmaceuticals* 2022;**15**:1021.
85. Ghahremanpour MM, Tirado-Rives J, Deshmukh M, Ippolito JA, Zhang CH, Cabeza de Vaca I, et al. Identification of 14 known drugs as inhibitors of the main protease of SARS-CoV-2. *ACS Med Chem Lett* 2020;**11**:2526–33.
86. Zhang CH, Stone EA, Deshmukh M, Ippolito JA, Ghahremanpour MM, Tirado-Rives J, et al. Potent noncovalent inhibitors of the main protease of SARS-CoV-2 from molecular sculpting of the drug peramppanel guided by free energy perturbation calculations. *ACS Cent Sci* 2021;**7**:467–75.
87. Zhang CH, Spasov KA, Reilly RA, Hollander K, Stone EA, Ippolito JA, et al. Optimization of triarylpyridinone inhibitors of the main protease of SARS-CoV-2 to low-nanomolar antiviral potency. *ACS Med Chem Lett* 2021;**12**:1325–32.
88. Deshmukh MG, Ippolito JA, Zhang CH, Stone EA, Reilly RA, Miller SJ, et al. Structure-guided design of a peramppanel-derived pharmacophore targeting the SARS-CoV-2 main protease. *Structure* 2021;**29**:823–833.e5.
89. Turlington M, Chun A, Tomar S, Egger A, Stauffer SR. Discovery of *N*-(benzo[1,2,3]triazol-1-yl)-*N*-(benzyl) acetamido)phenyl) carboxamides as severe acute respiratory syndrome coronavirus (SARS-CoV) 3CLpro inhibitors: identification of ML300 and noncovalent nanomolar inhibitors with an induced-fit binding. *Bioorg Med Chem Lett* 2013;**23**:6172–7.
90. Han SH, Goins CM, Arya T, Shin WJ, Maw J, Hooper A, et al. Structure-based optimization of ML300-derived, noncovalent inhibitors targeting the severe acute respiratory syndrome coronavirus 3CL protease (SARS-CoV-2 3CLpro). *J Med Chem* 2022;**65**:2880–904.
91. Douangamath A, Fearon D, Gehrtz P, Krojer T, Lukacik P, Owen CD, et al. Crystallographic and electrophilic fragment screening of the SARS-CoV-2 main protease. *Nat Commun* 2020;**11**:5047.
92. Gao S, Sylvester K, Song L, Claff T, Jing L, Woodson M, et al. Discovery and crystallographic studies of trisubstituted piperazine derivatives as non-covalent SARS-CoV 2 main protease inhibitors with high target specificity and low toxicity. *J Med Chem* 2022;**65**:13343–64.
93. Unoh Y, Uehara S, Nakahara K, Nobori H, Yamatsu Y, Yamamoto S, et al. Discovery of S-217622, a noncovalent oral SARS-CoV-2 3CL protease inhibitor clinical candidate for treating COVID-19. *J Med Chem* 2022;**65**:6499–512.
94. Tyndall JDA. S-217622, a 3CL protease inhibitor and clinical candidate for SARS-CoV-2. *J Med Chem* 2022;**65**:6496–8.
95. Nobori H, Fukao K, Kuroda T, Anan N, Tashima R, Nakashima M, et al. Efficacy of ensitrelvir against SARS-CoV-2 in a delayed-treatment mouse model. *J Antimicrob Chemother* 2022;**77**:2984–91.
96. Sasaki M, Tabata K, Kishimoto M, Itakura Y, Kobayashi H, Ariizumi T, et al. S-217622, a SARS-CoV-2 main protease inhibitor, decreases viral load and ameliorates COVID-19 severity in hamsters. *Sci Transl Med* 2023;**15**:eabq4064.
97. Shionogi. Shionogi presents phase 2/3 clinical trial results (Phase 2a Part) for the COVID-19 therapeutic drug S-217622. Available from: <https://www.shionogi.com/global/en/news/2022/2/e-20220207.html>.
98. Shionogi. Shionogi announces achievement of the primary endpoint for ensitrelvir fumaric acid (S-217622) in the phase 3 part of the phase 2/3 clinical trial in Asia. Available from: <https://www.shionogi.com/global/en/news/2022/09/20220928.html>.
99. Li Q, Kang C. Perspectives on fragment-based drug discovery: a strategy applicable to diverse targets. *Curr Top Med Chem* 2021;**21**:1099–112.
100. Pearce NM, Krojer T, Bradley AR, Collins P, Nowak RP, Talon R, et al. A multi-crystal method for extracting obscured crystallographic states from conventionally uninterpretable electron density. *Nat Commun* 2017;**8**:15123.
101. Bajusz D, Wade WS, Satala G, Bojarski AJ, Ilaš J, Ebner J, et al. Exploring protein hotspots by optimized fragment pharmacophores. *Nat Commun* 2021;**12**:3201.
102. Cantrelle FX, Boll E, Brier L, Moschidi D, Belouzard S, Landry V, et al. NMR spectroscopy of the main protease of SARS-CoV-2 and fragment-based screening identify three protein hotspots and an antiviral fragment. *Angew Chem Int Ed Engl* 2021;**60**:25428–35.
103. The COVID Moonshot Consortium. Open science discovery of oral non-covalent SARS-CoV-2 main protease inhibitor therapeutics. *bioRxiv* 2022. Available from: <https://doi.org/10.1101/2020.10.29.339317v3>.
104. Saar KL, McCorkindale W, Fearon D, Boby M, Barr H, Ben-Shmuel A, et al. Turning high-throughput structural biology into predictive inhibitor design. *Proc Natl Acad Sci U S A* 2023;**120**:e2214168120.
105. Morris A, McCorkindale W, Consortium TCM, Drayman N, Chodera JD, Tay S, et al. Discovery of SARS-CoV-2 main protease inhibitors using a synthesis-directed de novo design model. *Chem Commun* 2021;**57**:5909–12.
106. PostEra. COVID Moonshot. Available from: <http://postera.ai/covid>.
107. Bray S, Dudgeon T, Skyner R, Backofen R, Grüning B, von Delft F. Galaxy workflows for fragment-based virtual screening: a case study on the SARS-CoV-2 main protease. *J Cheminf* 2022;**14**:22.
108. Li J, Zhou X, Zhang Y, Zhong F, Lin C, McCormick PJ, et al. Crystal structure of SARS-CoV-2 main protease in complex with the natural product inhibitor shikonin illuminates a unique binding mode. *Sci Bull* 2021;**66**:661–3.
109. Su HX, Yao S, Zhao WF, Li MJ, Liu J, Shang WJ, et al. Anti-SARS-CoV-2 activities in vitro of Shuanghuanglian preparations and bioactive ingredients. *Acta Pharmacol Sin* 2020;**41**:1167–77.
110. Abian O, Ortega-Alarcon D, Jimenez-Alesanco A, Ceballos-Laita L, Vega S, Reyburn HT, et al. Structural stability of SARS-CoV-2 3CL^{Pro} and identification of quercetin as an inhibitor by experimental screening. *Int J Biol Macromol* 2020;**164**:1693–703.

111. Mangiacavalli F, Botwina P, Menichetti E, Bagnoli L, Rosati O, Marini F, et al. Seleno-functionalization of quercetin improves the non-covalent inhibition of M^{Pro} and its antiviral activity in cells against SARS-CoV-2. *Int J Mol Sci* 2021;**22**:7048.
112. Baell J, Walters MA. Chemistry: chemical con artists foil drug discovery. *Nature* 2014;**513**:481–3.
113. Lee CC, Kuo CJ, Ko TP, Hsu MF, Tsui YC, Chang SC, et al. Structural basis of inhibition specificities of 3C and 3C-like proteases by zinc-coordinating and peptidomimetic compounds. *J Biol Chem* 2009;**284**:7646–55.
114. Panchariya L, Khan WA, Kuila S, Sonkar K, Sahoo S, Ghoshal A, et al. Zinc²⁺ ion inhibits SARS-CoV-2 main protease and viral replication *in vitro*. *Chem Commun* 2021;**57**:10083–6.
115. Tao X, Zhang L, Du L, Lu K, Zhao Z, Xie Y, et al. Inhibition of SARS-CoV-2 replication by zinc gluconate in combination with hinokitiol. *J Inorg Biochem* 2022;**231**:111777.
116. Johansen-Leete J, Ullrich S, Fry SE, Frkic R, Bedding MJ, Aggarwal A, et al. Antiviral cyclic peptides targeting the main protease of SARS-CoV-2. *Chem Sci* 2022;**13**:3826–36.
117. Alzyoud L, Ghattas MA, Atareh N. Allosteric binding sites of the SARS-CoV-2 main protease: potential targets for broad-spectrum anti-coronavirus agents. *Drug Des Dev Ther* 2022;**16**:2463–78.
118. Günther S, Reinke PYA, Fernández-García Y, Lieske J, Lane TJ, Ginn HM, et al. X-ray screening identifies active site and allosteric inhibitors of SARS-CoV-2 main protease. *Science* 2021;**372**:642–6.
119. El-Baba TJ, Lutomski CA, Kantsadi AL, Malla TR, John T, Mikhailov V, et al. Allosteric inhibition of the SARS-CoV-2 main protease: insights from mass spectrometry based assays. *Angew Chem* 2020;**132**:23750–4.
120. Boggetto N, Reboud-Ravaux M. Dimerization inhibitors of HIV-1 protease. *Biol Chem* 2002;**383**:1321–4.
121. Goyal B, Goyal D. Targeting the dimerization of the main protease of coronaviruses: a potential broad-spectrum therapeutic strategy. *ACS Comb Sci* 2020;**22**:297–305.
122. Liang J, Karagiannis C, Pitsillou E, Darmawan KK, Ng K, Hung A, et al. Site mapping and small molecule blind docking reveal a possible target site on the SARS-CoV-2 main protease dimer interface. *Comput Biol Chem* 2020;**89**:107372.
123. Sztain T, Amaro R, McCammon JA. Elucidation of cryptic and allosteric pockets within the SARS-CoV-2 main protease. *J Chem Inf Model* 2021;**61**:3495–501.
124. Owen DR, Allerton CMN, Anderson AS, Aschenbrenner L, Avery M, Berritt S, et al. An oral SARS-CoV-2 M^{Pro} inhibitor clinical candidate for the treatment of COVID-19. *Science* 2021;**374**:1586–93.
125. Hoffman RL, Kania RS, Brothers MA, Davies JF, Ferre RA, Gajiwala KS, et al. Discovery of ketone-based covalent inhibitors of coronavirus 3CL proteases for the potential therapeutic treatment of COVID-19. *J Med Chem* 2020;**63**:12725–47.
126. Hao GF, Wang F, Li H, Zhu XL, Yang WC, Huang LS, et al. Computational discovery of picomolar Q(o) site inhibitors of cytochrome bc1 complex. *J Am Chem Soc* 2012;**134**:11168–76.
127. Hao GF, Jiang W, Ye YN, Wu FX, Zhu XL, Guo FB, et al. ACFIS: a web server for fragment-based drug discovery. *Nucleic Acids Res* 2016;**44**:W550–6.
128. Lambrinidis G, Tsantili-Kakoulidou A. Multi-objective optimization methods in novel drug design. *Expert Opin Drug Discov* 2021;**16**:647–58.
129. Chamakuri S, Lu S, Ucisik MN, Bohren KM, Chen YC, Du HC, et al. DNA-encoded chemistry technology yields expedient access to SARS-CoV-2 M^{Pro} inhibitors. *Proc Natl Acad Sci U S A* 2021;**118**:e2111172118.
130. Sutanto F, Shaabani S, Oerlemans R, Eris D, Patil P, Hadian M, et al. Combining high-throughput synthesis and high-throughput protein crystallography for accelerated hit identification. *Angew Chem Int Ed Engl* 2021;**60**:18231–9.
131. Wang X, Huang B, Liu X, Zhan P. Discovery of bioactive molecules from CuAAC click-chemistry-based combinatorial libraries. *Drug Discov Today* 2016;**21**:118–32.
132. Sarkar A, Mandal K. Repurposing an antiviral drug against SARS-CoV-2 main protease. *Angew Chem Int Ed Engl* 2021;**60**:23492–4.
133. Schuller M, Correy GJ, Gahbauer S, Fearon D, Wu T, Díaz RE, et al. Fragment binding to the Nsp3 macrodomain of SARS-CoV-2 identified through crystallographic screening and computational docking. *Sci Adv* 2021;**7**:eabf8711.
134. Newman JA, Douangamath A, Yadzani S, Yosaatmadja Y, Aimon A, Brandão-Neto J, et al. Structure, mechanism and crystallographic fragment screening of the SARS-CoV-2 NSP13 helicase. *Nat Commun* 2021;**12**:4848.
135. Schönherr H, Cernak T. Profound methyl effects in drug discovery and a call for new C–H methylation reactions. *Angew Chem Int Ed Engl* 2013;**52**:12256–67.
136. Chiodi D, Ishihara Y. Magic chloro: profound effects of the chlorine atom in drug discovery. *J Med Chem* 2023;**66**:5305–31.
137. Zhang X, Xu S, Sun L, Ding D, Tao Y, Kang D, et al. HIV-1 capsid inhibitors: a sword to destroy the virus. *Future Med Chem* 2022;**14**:605–7.
138. Ozen A, Haliloğlu T, Schiffer CA. HIV-1 protease and substrate coevolution validates the substrate envelope as the substrate recognition pattern. *J Chem Theor Comput* 2012;**8**:703–14.
139. Shen Y, Altman MD, Ali A, Nalam MN, Cao H, Rana TM, et al. Testing the substrate-envelope hypothesis with designed pairs of compounds. *ACS Chem Biol* 2013;**8**:2433–41.
140. Shaqra AM, Zvornicanin SN, Huang QYJ, Lockbaum GJ, Knapp M, Tandeske L, et al. Defining the substrate envelope of SARS-CoV-2 main protease to predict and avoid drug resistance. *Nat Commun* 2022;**13**:3556.
141. Flynn JM, Samant N, Schneider-Nachum G, Barkan DT, Yilmaz NK, Schiffer CA, et al. Comprehensive fitness landscape of SARS-CoV-2 M^{Pro} reveals insights into viral resistance mechanisms. *Elife* 2022;**11**:e77433.
142. Lee JT, Yang Q, Gribenko A, Perrin Jr BS, Zhu Y, Cardin R, et al. Genetic surveillance of SARS-CoV-2 M^{Pro} reveals high sequence and structural conservation prior to the introduction of protease inhibitor Paxlovid. *mBio* 2022;**13**:e0086922.
143. Zhang J, Peng X, Or YS. *Novel macrocyclic antiviral agents*. WO2022235605A1. 2022.
144. Yamini G, Nestorovich EM. Multivalent inhibitors of channel-forming bacterial toxins. *Curr Top Microbiol Immunol* 2017;**406**:199–227.
145. Ma Y, Frutos-Beltrán E, Kang D, Pannecouque C, De ClercqE, Menéndez-Arias L, et al. Medicinal chemistry strategies for discovering antivirals effective against drug-resistant viruses. *Chem Soc Rev* 2021;**50**:4514–40.
146. De Wispelaere M, Du G, Donovan KA, Zhang T, Eleuteri NA, Yuan JC, et al. Small molecule degraders of the hepatitis C virus protease reduce susceptibility to resistance mutations. *Nat Commun* 2019;**10**:3468.
147. Liang JS, Wu YH, Lan K, Dong C, Wu SW, Li S, et al. Antiviral PROTACs: opportunity borne with challenge. *Cell Insight* 2023;**2**:100092.
148. Liang C, Xin L, Tian L, Xia J, Qin N, Li J, et al. *PROTACS targeting coronavirus 3CL protease and preparation method and application thereof*. US 11530195 B1. 2023.